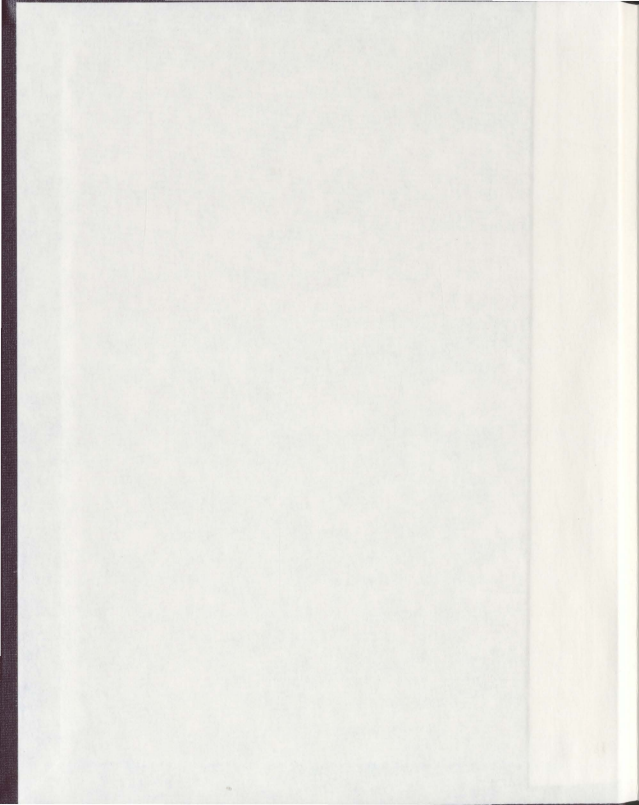# FORECASTING SPATIO-TEMPORAL VEGETATION CHANGES IN THE MEALY MOUNTAINS USING A CELLULAR AUTOMATA-MARKOV CHAIN HYBRID MODEL

ZACHARY BARTLETT

FORECASTING SPATIO-TEMPORAL VEGETATION

CHANGES IN THE MEALY MOUNTAINS USING A

CELLULAR AUTOMATA-MARKOV CHAIN

HYBRID MODEL

BY

© ZACHARY BARTLETT

A thesis submitted to the
School of Graduate Studies
in partial fulfilment of the
requirements for the degree of
Master of Science

Department of Geography
Memorial University of Newfoundland

December 2011

ABSTRACT

Sub-arctic temperatures are expected to increase by approximately 4° C by 2050. These changes are having impacts on vegetation patterns in arctic and sub-arctic environments, particularly along transition areas between forested and tundra ecosystems. Using multi-temporal satellite imagery, in combination with topographic variables, the changes in vegetation patterns from 1983 to 2008 were explored in a small, diverse region of the Mealy Mountains, Labrador. Bayesian probabilities were created for each land cover class, with topographic variables used as *a priori* additions to the probabilities. Vegetation changes were related to topographic variables, climate, and Bayesian probabilities. The Bayesian probability layers demonstrate the propensity for change of each land cover class used in the study. Knowledge of these changes was used in a cellular automata-Markov chain model to predict vegetation changes to 2020 and 2032. The predictions suggest movement of deciduous shrub along valley floors and into toe-slopes, as well as on protected, south-facing slopes. Coniferous shrub is expected to expand in the lower elevations (where it is dominant), and advance marginally along the valley floors.

ACKNOWLEDGEMENTS

CONTENTS

LIST OF TABLES

LIST OF FIGURES

LIST OF EQUATIONS

LIST OF ABREVIATIONS

BRK: Bedrock/exposed

CA: Cellular Automata

CA-Markov: Cellular Automata-Markov Chain

CSH: Coniferous Shrub

DSH: Deciduous Shrub

ECI: Elevation - % Cover Index

HTH: Heath

KIA: Kappa Index of Agreement (κ)

OLS: Ordinary Least Squares

PCQ: Point-Centre Quarter

RMSE: Root-Mean Square Error

SWness: Southwestness

TCI: TSI - % Cover Index

TRMI: Topographic Relative Moisture Index

TSI: Topographic Shape Index

LIST OF APPENDICES

1. INTRODUCTION

1.1 Nature and rationale

The Intergovernmental Panel on Climate Change predicts that global temperatures are changing at an increasingly rapid pace (IPCC, 2007). Under these conditions, significant shifts are expected to occur in vegetation patterns, particularly in sensitive 'edge' ecosystems such as at the tree line, which forms the boundary between the boreal forest and the treeless arctic tundra, also known as the forest-tundra ecotone (Gamache and Payette, 2005). Future climate scenarios established by the Canadian Institute for Climate Studies (CICS) suggests warming of up to 4° C in sub-arctic regions over the next several decades (Figure 1.1).

Payette (2007) states that, in general, North American boreal forest tree lines have moved up-slope and northward over the past 100 years, and are expected to do so under changing climatic conditions.

Considerable research has been completed on the effects of a changing climate on vegetation patterns and tree line shifts in arctic and sub-arctic environments (Payette and Delwaide, 1994; Lloyd and Fastie, 2002; Körner and Paulsen, 2004; MacDonald *et al.*, 2008). Carmel and Kadmon (2008), however, suggest that these studies are situated over large geographic areas (*i.e.* several hundred km^2) and short time frames (*e.g.* <10 years). These restrictions limit the level of detail frequently desirable in vegetation studies. In addition, studies suggest that significant climatic shifts occur over decadal time frames (Pereg and Payette, 1998; Epstein *et al.*, 2004; Stow *et al.*, 2004; IPCC, 2007) and so statistically significant changes would be less reliable with data spanning less than 10

CGCM2 A21 (SRES) - Annual - Mean Temperature Change - 2050s   Prepared by CCIS Project
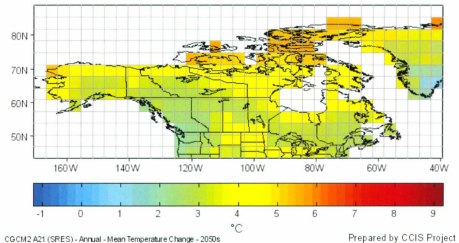
Figure 1.1 Predicted annual mean temperature change to 2050s (Canadian Institute for Climate Studies, 2003)

years. This study addresses these shortcomings by focusing on a small geographic area (~100 km^2) over a relatively large time frame (approximately 25 years) in an effort to understand past and future vegetation changes in the Mealy Mountains of Labrador. This approach ensures a high level of detail in land cover changes, as well as retaining statistically significant climate shifts.

1.2 Study area

The study area is located in the Mealy Mountains of Labrador approximately 100 km southeast of the town of Happy Valley-Goose Bay, within the boundaries of the Mealy Mountains (*Akamiuapishku*) National Park. Figure 1.2 outlines the study area. The extent of the study area ranges from approximately 53.632° N, 58.895° W in the northwest corner to 53.563° N, 58.780° W in the southeast corner, covering an area approximately

10 km X 10 km. The elevation ranges from about 450 m to 1000 m. This area is unique in that the lower elevations (450-750 m) exhibit considerably different vegetation patterns than the higher elevations (>750 m). Figure 1.3 and 1.4 highlight the topographic conditions of Labrador and a small scale view of the study area, respectively. The landscape in the study area is characterised by rolling valleys and hills. However, near the summit, steeper slopes are prominent. Figure 1.5 shows a topographic profile of the study area.

At lower elevations (~400-500 m), the forest-tundra ecotone is composed of black spruce (*Picea mariana*) and eastern larch (*Larix laricina*), which form a largely open canopy forest cover type, with a primarily moss understory. As with most tree lines, the limit of tree growth in the Mealy Mountains is marked by a gradual decrease in tree height and density. Moving upslope, trees become shorter and more spread out. This transition occurs in the mid-range elevations (~500-700 m), where upright trees are replaced by more dwarfed krummholz (low-lying coniferous shrubs stunted by environmental factors). At these elevations, a higher occurrence of ericaceous shrubs is be found as well, such a Labrador tea (*Rhodendron tomentosum*), bearberry (*Arctostaphylos uva-ursi*), dwarf bilberry (*Vaccinium uliginosum*), and sheep laurel (*Kalmia angustifolia*). Farther upslope dwarf birch (*Betula glandulosa*) and speckled alder (*Alnus rugosa*) also become abundant.

At higher elevations (>700 m), trees and krummholz are nearly non-existent. Instead the vegetation cover is dominated by stunted forms of the species found in the mid-range elevations, with the exception of speckled alder. In addition, diapensia

3

(*Diapensia laponica*), black crowberry (*Empetrum nigrum*), and an abundance of mosses and lichens are present.
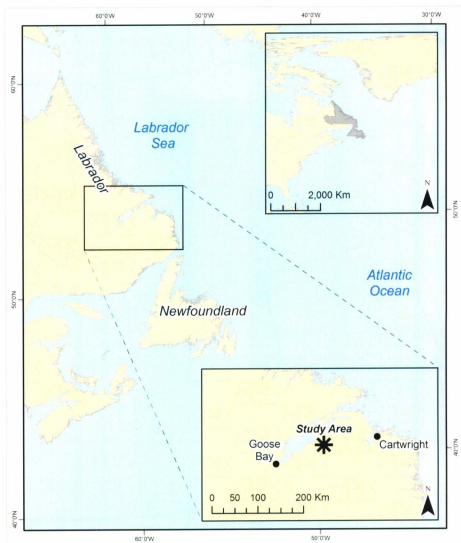
Figure 1.2 Outline of the general study in relation to North America
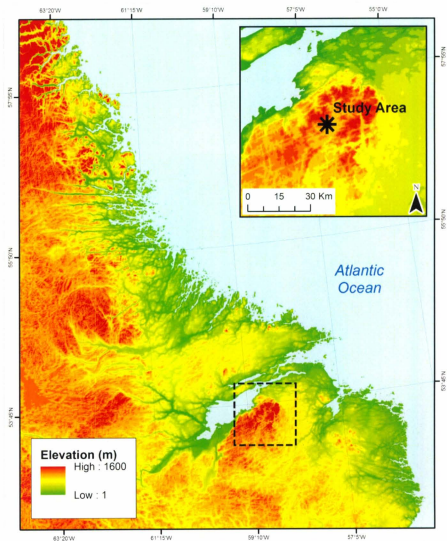
Figure 1.3 Outline of the study area in relation to the topography of Eastern Labrador
(Source: Shuttle Radar Topography Mission, United States Geological Survey, 2010)
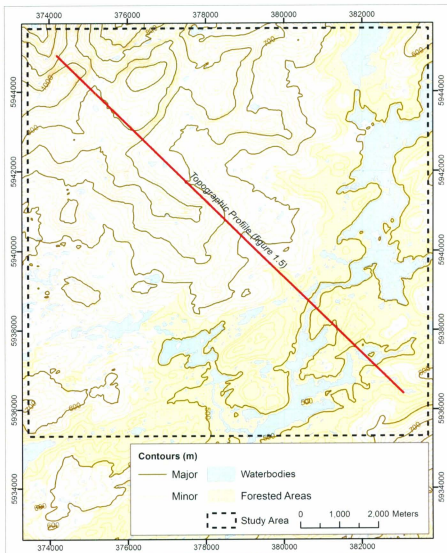
Figure 1.4 Detailed overview of study area (Source: Natural Resources Canada, 2010)
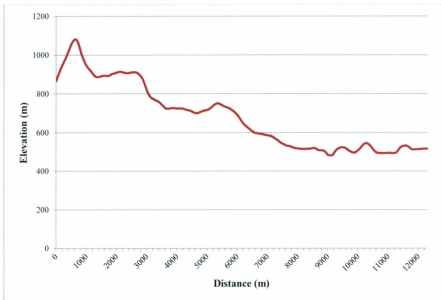
Figure 1.5 Topographic profile of Mealy Mountains study area

Tree-ring analysis in the area confirms the occurrence of several forest fires over the past 100 years. However, they were all localised events and had little effect on vegetation trends (Jacobs, 2007). There were no other recorded disturbances in the area.

Climate variability in the region is strongly associated with variability in the Icelandic Low. This produces damp conditions, leading to large amounts of snow which usually remains into the late summer months. In the summer, low pressure over Ungava Bay brings westerly winds to the region (Keith, 2001). Environment Canada (2009) climate data for Goose Bay and Cartwright show an increase of approximately 1.2° from 1983-2001, with a more pronounced increase of 1.0° C from 2001-2008 (Figure 1.6). The Canadian Institute of Climate Studies (2003) predicts a mean increase in summer

temperature of 2.5º C by the 2020s, and an increase of 3.9º C by the 2050s, from current climate normals.
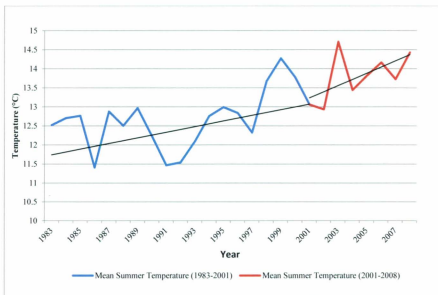
Figure 1.6 Mean summer temperature (1983-2001) with trendline

1.3 Purpose and objectives

The purpose of this study is to attain a better understanding of the effects of climate and topography on vegetation patterns, distributions, and movements. It expands on the body of research devoted to spatial-temporal modelling of vegetation. In a broader spectrum, the research complements the goals of the International Polar Year (IPY) research (2005).

The objectives of this study are to:

1. Create vegetation maps of historical land cover distributions;

2. Understand how land cover has changed given past climate fluctuations by
    comparing land cover distributions with known climate shifts;

3. Identify topographic conditions specific to the different land cover classes to
    aid in the development of a spatio-temporal forecasting model; and

4. Run a cellular automata-Markov chain model to forecast future land cover
    conditions as well as understand historic shifts in land cover.

1.4 Theory and assumptions

The dominant theory in vegetation and treeline studies is that, under warming conditions

in northern environments, treelines and shrub biomes (deciduous and coniferous) are

expected to move upslope and northward (Gamache and Payette, 2005; Payette, 2007).

Treelines and biome boundaries, however, are not easily discernable because the

transition between the forested regions at lower elevations and the treeless, arctic tundra

at higher elevations is marked by a gradual decrease in tree density and size. Moving

upslope, trees become more sporadic, forming as krummholz.

An important assumption that must be made when examining vegetation change is

that climate and topography are strongly associated with vegetation shifts. Many

researchers agree that plant migration likely lags behind climate warming, resulting in

disequilibrium between climate and vegetation distributions (Huntley, 1991; Malcolm *et

al.*, 2002). However, in order to accurately develop correlation measures between the

variables used in the model, one must make the assumption that the time frame from

which these statistics are being extracted was in an equilibrium state. For the purposes of

model development, this assumption is being violated and it is assumed that the

environment was not in a state of flux at the time the satellite images were captured

(Huntley, 1991; Malcolm *et al.*, 2002).

1.5 Context of research

This research was conducted as part of the International Polar Year research initiative.

The objectives of the IPY that are relevant to this study are:

1. "Utilise the vantage point of the polar regions to carry out an intensive and internationally coordinated burst of high quality, important research activities and observations that would not otherwise occur;

2. Lay the foundation for major scientific advances in knowledge and understanding of the nature and behaviour of the polar regions and their role in the functioning of the planet;

3. Collect a broad-ranging set of samples, data and information regarding the state and behaviour of the polar regions to provide a reference for comparison with the future and the past; and

4. Intensify the recovery of relevant historical data and ensure that these also are made openly available." (IPY, 2005)

2. LITERATURE REVIEW

This section presents an overview of the current literature regarding the influence of topographic variables on vegetation patterns (section 2.1). Climate interpolation and change detection are discussed in sections 2.2 and 2.3, respectively. Section 2.4 discusses how Bayesian probabilities have been used in a range of studies and how they are adapted to ecological modelling. Sections 2.6, 2.7, and 2.8 present a synopsis of the modelling techniques that will be used in this study.

2.1 Topographic variables

Temperature plays an important role in the position and movement of vegetation and ecotones. However, topography can sometimes be an inhibitor or promoter of vegetation shifts. Rupp *et al*. (2001) found that the "interaction between topography, climate, and disturbance could alter patterns to reduce or offset current predicted positive feedbacks to warming at high latitudes." Their results indicated that topography played a major role in constraining the movement of the boreal forest into treeless areas, whereby the Brooks Range in Alaska was found to be an environmental barrier to forest expansion (Rupp *et al*., 2001).

Treml and Banaš (2008) studied the effects of exposure on alpine treeline position. They found that the highest positions of the treeline were generally distributed on slopes receiving higher heat loads. Surfaces facing in the southwest direction generally receive more sunlight, thus more direct heating. Therefore, given sufficient levels of precipitation, seedlings are more likely to survive. This implies a faster upward

11

shift of the treeline on favourable aspects as a consequence of these generally warmer temperatures (Treml and Banaš, 2008).

Holland and Steyn (1975) state that the effect of aspect varies with latitude. With a higher sun-angle (*i.e.* those near the equator) the radiant energy incident upon a north- or east-facing slope would be greater than those areas with a low sun-angle (*i.e.* those at higher latitudes). The authors state that the effects of aspect are most prominent at 45° latitude or greater north and south of the equator (Holland and Steyn, 1975). The Mealy Mountains study area is centered at approximately 53.5° N, an area where the effects of aspect would be significant.

Aspect is a circular measurement, with values ranging from 0° to 360°. However, while there is a considerable numerical difference between 2° and 358°, on the ground they are both north-facing. Therefore, Miller (2005) developed the concept of "southwestness." Southwestness is a scalar measurement ranging from -1 to 1. Perfectly southwest-facing slopes (considered the most favourable for growth) receive values of 1. As the aspect moves farther from southwest, the values decrease. A northeast-facing slope is coded as -1. All values in between (*e.g.* northwest, southeast, east, *etc.*) would fall somewhere within the two extremes.

2.2 Climate data interpolation

When climate data are not available for a particular study area, there are methods used to interpolate these values. Hanson (1987) uses linear regression to determine the mass balance of a glacier from known temperatures at a nearby weather station. The researchers' goal was to develop a long-running record of glacial mass balance; however,

only 17 years of mass balance data were available. A climate station located 120 km away had continuous weather measurements covering the entire time frame of interest. Regression was performed between the climate station's mean summer temperatures and the glacial mass balance. Hanson (1987) found high negative correlations between the climate data, particularly mean summer temperatures, and the observed glacier mass balance.

The methodology outlined in the preceding study was adapted for two climate stations at Goose Bay and Cartwright to interpolate climate conditions at the Mealy Mountains study area. The results of this analysis are presented in Chapter 3.

2.3 Change detection

Historic land cover conditions provide useful information regarding vegetation trends. When developing a model to predict potential future conditions, it is important to be aware of these changes, as they are used to calibrate the model.

The use of multi-temporal satellite imagery permits the long-term monitoring of vegetation changes. These changes are usually evident over decadal time scales (Epstein *et al.,* 2004). Jano *et al.* (1998) used Landsat imagery from 1973, 1984, and 1993 to examine changes in vegetation patterns due to herbivore foraging. The authors noted that in order to avoid confusing seasonal changes in vegetation with long-term fluctuations, it is preferable to obtain imagery recorded at times when the development of vegetation is at identical or very similar stages. Thus, late-summer provides the ideal time frame for image acquisition. During this period, different vegetation types are expected to be in

similar growth stages, and have yet to experience the colder fall temperatures which decrease photosynthetic activity.

Change detection techniques work with two types of data: qualitative and quantitative. For example, a land cover map showing several discrete classes of vegetation is considered qualitative. A Normalized Difference Vegetation Index (NDVI) would represent quantitative data (Myneni *et al.*, 1995; Stow *et al.*, 2004; Jensen, 2005).

Eastman (2009) lists several change detection techniques for both types of data. For qualitative data, a crosstabulation is often performed, where the number of pixels that change from one class to another are tallied. Values along the diagonal of the matrix (whose rows and columns represent the classes of the images, which must be identical) represent no change in land cover types. The off-diagonal values represent transitions from one class to another. A Kappa Index of Agreement (KIA) generally accompanies a crosstabulation. This value, computed for the whole image and also for each class in the image, represents the level of agreement between the two images. If considerable change has occurred, the Kappa value will be low, representing a low level of agreement between the images. The per class Kappa values tend to be more useful as they show the level of agreement within each land class; so if an overall Kappa is low, one or more of the per class Kappa values may still be high, indicating some level of persistence.

When data are in a quantitative form, such as an NDVI image, there are several different methods that can be utilized. The most common, and usually most informative, is image differencing (Byrne *et al.*, 1980; Hayes *et al.*, 2001). This technique involves

14

subtracting images from two different dates. Often, the raw difference values are extremely high or low. Therefore, it is recommended to normalize these values as a percent change (later-earlier/earlier), a standardized image (z-score), or a classified standardized image (z-scores divided into classes).

2.4 Bayesian probabilities

When combining datasets, the Bayesian approach uses a probability framework to represent the data portrayed from multiple sources. The Bayesian method works with the notion of prior and posterior probabilities (Bonham-Carter, 1994). Given a continuous area of vegetation over a known geographic space, a prior probability would be the likelihood of finding a particular land cover at a given time, based solely on the proportions of different land covers currently in the defined space. The prior probability of finding a particular land cover, in this case, is the ratio of the area of that land cover to the total area of the study site. Posterior probabilities are calculated by adding predictive variables to the prior probability.

Borsuk *et al.*, (2006) used a Bayesian probability framework to analyse the decline of brown trout in Swiss rivers. They introduced variables such as gravel bed conditions, water quality and temperature, disease rates, and habitat conditions to develop posterior probabilities. Caley *et al.*, (2008) adapted a similar technique for estimating the success of introduced plants. They combined prior estimates of the probability of naturalisation and the time from introduction to naturalisation. The authors conclude that estimating the success rate of introduced plants and ignoring the prior estimates results in high success rates, however, their estimates were very uncertain. Introducing the prior

estimates into the probability framework decreased the calculated success rate and the uncertainty associated therein.

2.5 Markov chains

Markov chains provide the propensity for a particular state to transition to another state in the system (Collins, 1975). This methodology can be applied to vegetation studies, where a particular state could be, for example, a land cover, and a system is made up of several land cover classes.

A Markov chain is a stochastic process with deterministic elements. Generally speaking, a stochastic process is defined as one which provides the probability associated with a set of possible future outcomes. In a deterministic process, state X is always followed by state Y. However, in a stochastic process, state X is followed by state Y, with a probability p, and by state Z with a probability $q = 1 - p$ (Collins, 1975).

A process is deemed Markovian when it fulfills the Markov property. According to Logofet and Lesnaya (2000), "if the chain is in a state i at a given time moment s, then the probability $p_{ij}(s,t)$ that it will be in a state j at a subsequent time instant $t>s$ does not depend on the chain behaviour before the moment s." Thus, the state of a system at a given time depends on the state of the system at the time period prior to it, but no further into the past. In this situation, the process is considered a first-order Markov chain.

The order of a Markov chain dictates the influence of past events on the current event. At time $t(0+1)$, the state of the system is dependent on the state at time $t(0)$, plus some other random function. This is referred to as a first-order Markov chain. In a

second-order Markov chain, the state of the system at time $t(0+1)$ is dependent on the state at time $t(0)$ and time $t(0-1)$ (Collins, 1975).

A transition matrix, denoted P, with k possible states, is defined as:

$$P = \begin{bmatrix} p_{11} & p_{12} & \cdots & p_{1j} \\ p_{21} & p_{22} & \cdots & p_{2j} \\ \vdots & \vdots & \ddots & \vdots \\ p_{i1} & p_{i2} & \cdots & p_{ij} \end{bmatrix}$$

Equation 2.1 Markov transition matrix

Where:
P_{ij} = the probability of transitioning from state i to state j in the next time step.

The transition probabilities, p_{ij}, are given for every pair of states in the system. The probabilities must be non-negative, and all rows sum to 1. Over time, the Markov chain will reach equilibrium, where the number of entities in a system leaving a particular state is equal to the number going into that state, resulting in no change to the system with successive time steps (Collins, 1975).

There has been considerable work relating the application of Markov chains to vegetation succession and dynamics (Usher, 1981; Lippe *et al.*, 1985; Balzter, 2000; Logofet and Lesnaya, 2000; Benabdellah *et al.*, 2003). As with many ecological succession studies, certain assumptions must be made before an analysis can begin. Markov chains are no exception, and, as Balzter (2000) suggests, the prediction of future species (state) proportions makes the following assumptions:

- time-homogeneity,

- spatial dependence (influence on a species by neighbouring species),

- absence of colonisation by new species', and

- first-order Markov dependence

The issue of time-homogeneity refers to the period into the future that a Markov chain can forecast. This concept is more thoroughly explained by Logofet and Lesnaya (2000). The idea stems from the invariant environment hypothesis. In ecological terms, the invariance hypothesis means that:

> "no important changes [can] occur in the key factors of the environment affecting the course of succession during the period of prediction as compared with the factors during the period of observations in which estimation of the transition probabilities can be relied upon (Logofet and Lesnaya, 2000)."

This assumption of time-homogeneity in a Markov chain implies that transition probabilities can only be calculated into the future for T years, where T is the maximum number of years between the earliest and latest available observed data. This hypothesis also assumes that no major changes took place in the environment, such as disease, fire, or flooding. In the case of the Mealy Mountains study, the earliest imagery is 1983 while the latest is 2008. If following the time-homogeneity assumption and the invariance hypothesis, Markov chains can only be forecasted 25 years (2008-1983 = 25 years) into the future. After 25 years, the Markov transition probabilities become unreliable due to a lack of data.

The second point, spatial dependence, refers to the propensity for an object in space to be more like the objects near it. This is a fundamental concept in geography and spatial analysis. Markov chains deal with transitions between states over time, but do not

incorporate space. In other words, the spatial arrangement of the states in a system (if the system is in fact spatial) has no impact on the transition probabilities produced by the Markov chain. This is an issue which is accounted for by introducing other modelling techniques into the analysis, such as cellular automata (Section 2.6).

The third point outlined by Balzter (2000), the absence of colonisation by a new species, means that no new species' can be introduced into the model that were not present at time $t(0)$. The final point, first-order dependence, was discussed earlier in this section. In the context of this study, once a vegetation type occupies a space at time $t(n)$, and the next time step, $t(n+1)$, is analyzed, the vegetation types present at time $t(n-1)$ are no longer relevant. It is because of this that first-order Markov chains are suitable for vegetation studies (Balzter, 2000).

Given that the model used in this study is influenced heavily by Markov processes, these assumptions (time-homogeneity, spatial dependence, absence of colonisation, and first-order dependence) are important, and were considered carefully when developing the model, especially that of time-homogeneity. The issue of spatial dependence was addressed by introducing a cellular automata model.

2.6 Cellular automata

Cellular automata are gaining popularity in ecology due to their ability to incorporate spatial constraints on ecosystem development. Wolfram (1983) states that cellular automata "are used as simple mathematical models to investigate self-organization in statistical mechanics." They consists of a "sequence of sites with values 0 or 1[…] with each site evolving deterministically in discrete time steps according to definite rules

involving the values of its nearest neighbours." In other words, units in a system (*e.g.* pixels in a raster dataset) evolve based on the state of the units surrounding them.

The unique characteristic of cellular automata is that the state of a cell is dictated by the states of the cells in its neighbourhood and known transition rules. The most common neighbourhoods are the Moore-neighbourhood (consisting of the centre cell and its neighbouring eight cells) and the von Neumann-neighbourhood (consisting of the centre cell and its neighbouring four cells) (Figure 2.1) (Balzter *et al.*, 1998).
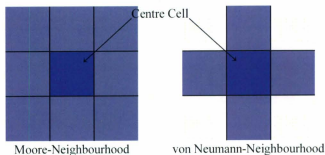
Figure 2.1 Most common cellular automata neighbourhoods (adopted from De Smith *et al.*, 2007)

While Figure 2.1 represents the most common cellular automata neighbourhoods, there are several other options available. The Idrisi Taiga (Eastman, 2009) software has a set neighbourhood; however, it can be modified by the user. Figure 2.2 shows the Idrisi Taiga cellular automata default search neighbourhood.

$$
\begin{array}{ccccc}
0 & 0 & \textcolor{red}{1} & 0 & 0 \\
0 & \textcolor{red}{1} & \textcolor{red}{1} & \textcolor{red}{1} & 0 \\
\textcolor{red}{1} & \textcolor{red}{1} & \textcolor{red}{1} & \textcolor{red}{1} & \textcolor{red}{1} \\
0 & \textcolor{red}{1} & \textcolor{red}{1} & \textcolor{red}{1} & 0 \\
0 & 0 & \textcolor{red}{1} & 0 & 0
\end{array}
$$

Figure 2.2 Idrisi Taiga cellular automata search neighbourhood

The purpose of a neighbourhood such as the one presented in Figure 2.2 is to provide a greater weight on neighbouring pixels than on more distant pixels. Observation of the neighbourhood reveals that the inner 3 x 3 block is the same as the Moore-Neighbourhood outlined above.

A simple cellular automaton, denoted A, is defined as:

$$A = <L, Q, \delta, f>$$

Equation 2.2 A simple cellular automaton

Where:
L = raster surface
Q = state space
δ = neighbourhood template
f = transition function

(Balzter *et al.*, 1998)

The transition rules can be either deterministic or stochastic (Czárán and Sándor, 1992), though stochastic rules have proven to perform better in ecological theory than deterministic rules (Phipps, 1992). The transition rules take the form:

$$a_{t+1}^s = f(a_t^{s-r}, \dots, a_t^s, \dots, a_t^{s+r})$$

Equation 2.3 Example of transition rule for cellular automata

21

Where:
a_t^s = state of the cell s at time t
r = range of the neighbourhood of cell s
f = local transition function representing the transition rules.

In ecological studies, particularly those dealing with vegetation, an unoccupied (*e.g.* dead) cell can become occupied (*e.g.* alive) if a certain number of its neighbours are already occupied. Conversely, the rules could be altered such that overcrowding (a target cell and a specified number of its neighbours are occupied) causes death. There is also the case of scarcity, in which an occupied target cell dies of 'loneliness' (*e.g.* lack of protection) when too few neighbours are present. For example, a particular vegetation class is likely to continuing advancing to new areas if all its neighbouring pixels are unoccupied or occupied by land covers susceptible to colonisation.

Cellular automata are discrete in time, space, and state, and can model processes at large scales (*e.g.* landscape dynamics) and small scales (*e.g.* single populations) (Balzter *et al.*, 1998). They forecast specific scenarios (states), at an exact point in time, over a spatially discrete area.

2.7 Cellular automata - Markov chain hybrid modelling

Markov chains have no spatial component. The influence of neighbouring features, thus, has no implicit impact on the transition of one state to another in Markov chain predictions. Cellular automata address this shortcoming. Markov chains and cellular automata algorithms can be integrated in most spatial analysis software. Such a coupling offers the advantage of an integrated environment which incorporates stochastic processes (from the Markov chain) with pre-determined rules (from the cellular automata)

concerning both the dynamics of a landscape and the spatial patterns present in the vegetation.

In the remote sensing and spatial modelling software program *IDRISI Taiga* (2009), the cellular automata-Markov chain model, or *CA_Markov* module, works in this manner. The module combines the following components to produce a prediction of land cover change:

- *Basis land cover image*: a map of the initial land cover state used;

- *Markov transition areas file*: transition areas derived from classified images used in the *Markov* module;

- *Transition suitability image collection*: set of images that show the suitability of transition for each individual land cover class;

- *Number of cellular automata iterations*: number of times the cellular automata repeats. This is the same value as the *Number of time periods to project forward from the second image* field in the *Markov* module (Eastman, 2009; Marshall and Randihir, 2008).

Generally, a test prediction would be made forward to a time with an observed land cover state. The predicted and observed land covers can then be compared in order to estimate the predictive power of the model (Eastman, 2009).

2.8 Summary of literature review

The literature presented in this section provide valuable insight into the techniques available for modelling past and future vegetation conditions. Topographic variables, such as aspect, elevation, and topographic shape, have a direct influence on the location and movement of vegetation, acting as both inhibitors and promoters of change. This knowledge allows one to more fully explore the relationships between land covers and

corresponding topographic characteristics. The topographic variables are used directly in the cellular automata-Markov chain model.

Climate is highly associated with the movement of vegetation over time. While it is not included in the model as a distinct variable, it is represented implicitly within the Markov chain projections as well as adiabatic rate layers within the Bayesian probabilities.

The Markov chain and cellular automata models provide the predictive tools used within this study. The coupling of the two provides an analysis which considers both time and space.

3. DATA SOURCES

This chapter presents the collection and processing of the field data (Section 3.1). The climate data are described in Section 3.2. Section 3.3 outlines the available aerial and satellite imagery and the processing steps performed in order to classify the images. Section 3.4 explains the generation of the topographic variables and how they were used to develop the Bayesian probabilities (Section 3.5).

3.1 Field data

In preparation for field work in 2008, sample points were generated based on random sampling stratified by elevation (derived from a digital elevation model (DEM)) and groundcover spectral signatures (derived from a high-resolution 2005 Quickbird satellite image). This stratification method was chosen to ensure a diversity of groundcovers were present in the field samples. Field work was carried out from 4 July to 20 July, 2008.

A total of 74 field points were collected (Figure 3.1). The X and Y coordinates of the collected samples are listed in Appendix A. At each of the sample points, five 1 m^2 quadrat samples were set up. Four quadrats were placed at a distance of 10 m from the centre point in the four primary cardinal directions. A fifth point, chosen randomly, was placed in either the northwest, northeast, southeast, or southwest direction (Chen *et al.*, 2007) (Figure 3.2). At each quadrat, the percent cover of all species' present was recorded. Average heights of each species and average soil depth were also recorded. A top-down photograph of each quadrat was taken using a digital camera. This protocol was applied in non-forested areas where vegetation is low-lying.
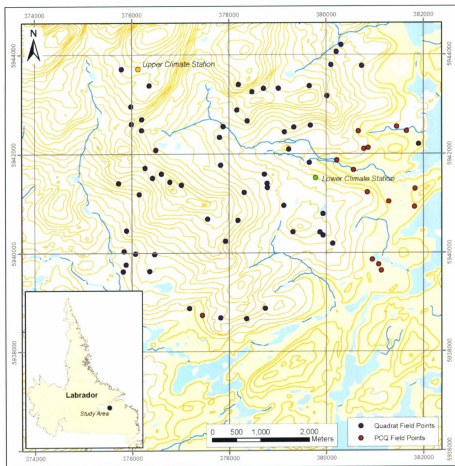
Figure 3.1 Sampling locations for field points, upper and lower climate station location
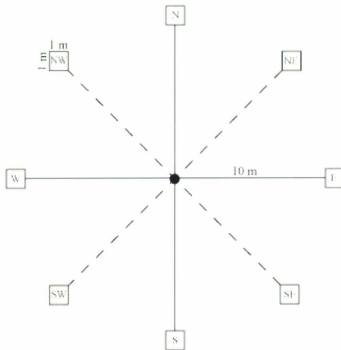
Figure 3.2 Quadrat Method applied to low-lying vegetation

Given that the data are arranged in groups of five points, interpreting dominant land covers would result in statistics highly influenced by clustering. Therefore, the mean of each quadrat was calculated to produce a value for each groundcover type present that was representative of the site. The result is a single quadrat with the average percentage cover of each recorded species; representing the conditions over a 20 m x 20 m area. The 18 groundcover classes were also grouped into land cover classes as developed by Meades (1990). The groups are as follows: tundra, krummholz, deciduous shrub, coniferous shrub, open canopy, closed canopy, understory, bedrock, water, and fen/bog.

Where tall trees were dominant, the Point-Center Quarter (PCQ) sampling scheme was used (Mitchell, 2007). This technique involves recording the distance to the closest tree of each species in four quadrants (NE, NW, SE, and SW) (Figure 3.3). At each tree, the basal diameter and the diameter at breast height (DBH) were recorded. Black spruce and eastern larch were the most abundant species' encountered, with sporadic occurrences of balsam fir (*Abies balsamia*) and white spruce (*Picea glauca*).
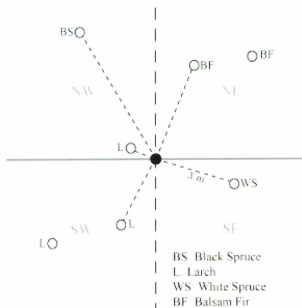
Figure 3.3 Point-Center Quarter (PCQ) method. Applied in forested areas. Note that only the nearest tree of each species was chosen per quadrant. (BS: Black Spruce; WS: White Spruce; BF: Balsam Fir; L: Larch)

Table 3.1 lists the different land cover types with general characteristics as well as a sample photograph. The classes used in the table correspond with those outlined by Meades (1990). However, the deciduous shrub and coniferous shrub classes have been excluded, as they are represented adequately by the open canopy and closed canopy classes.

Table 3.1 Land cover classes, composition, and sample images

Land Cover	Dominant Vegetation	Characteristics	Sample Image
Tundra	Labrador tea, crowberry, bearberry, kalmia, mosses, lichens	Low-lying vegetation, frequently interspersed with bedrock.	
Krummholz	White spruce, black spruce	Environmentally-stunted coniferous shrubs.	

Table 3.1 cont'd
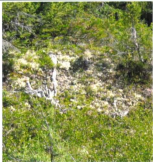
Land Cover	Dominant Vegetation	Characteristics	Sample Image
Open Canopy	Black spruce, white spruce, balsam fir, larch	Old growth forests with sparse canopy cover.	
Closed Canopy	Black spruce, white spruce, balsam fir, larch	Old growth forest with considerable canopy cover.	
Understory	Moss	Primarily located within old growth forests.	

30

Table 3.1 cont'd

Land Cover	Dominant Vegetation	Characteristics	Sample Image
Fen/Bog	Grasses, sedges	Usually wet areas dominated by sedges and rushes	
Bedrock	Exposed bedrock, boulders, shattered boulders	Interspersed with tundra vegetation. Primarily at higher elevations.	
Water		Waterbodies, seasonal and permanent.	

For the purposes of image classification, the above listed classes were grouped one step further into more manageable units. Using a supervised classification, the images were classified into one of four classes: deciduous shrub (DSH), coniferous shrub (CSH), heath (HTH), and bedrock/exposed (BRK). These four classes efficiently capture the vegetation types listed in Table 3.1. Additionally, Meades (1983) suggests that, given sufficient time, shrub classes will eventually over take the heath landcover. It should be

noted that the bedrock/exposed land cover classes represents areas with exposed bedrock, as well as exposed soil.

As will be discussed in Chapter 4, the heath and bedrock/exposed land covers occupy similar topographic conditions. In most cases, they are within close proximity to one another. This leads to pixel-mixing between the two land covers, whereby heath and bedrock/exposed occupy the same pixel. Thus, the spectral signature is skewed, making classification more difficult. This issue is confounded by the fact that heath and bedrock/exposed are very different in the infrared band. Figure 3.4 illustrates the spectral signatures of heath and bedrock/exposed. These values were extracted by selecting areas of both land covers form a high resolution Quickbird image.
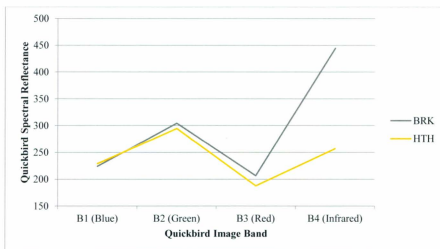
Figure 3.4 Spectral signatures of heath and bedrock/exposed

Pixel-mixing often results in misclassifications. This in turn results in potential errors in modelling. While these errors are unavoidable, it is important to be aware of them when analyzing results and forming conclusions.

3.2 Climate Data

3.2.1 Regional climate data

Historical climate data were obtained from Environment Canada (2009) for Goose Bay (1942-2008) and Cartwright (1941-2007). These data were used to interpolate climatic conditions for the Mealy Mountains based on the method outlined by Hanson (1987).

3.2.2 Local climate data

Climate data were collected for the study area from 17 July, 2001 to 8 July, 2007. Climate stations at 570 m and 1000 m (Figure 3.1) collected minimum, maximum and average temperature, as well as solar flux and ground temperature (Jacobs, 2007). These data represent local conditions, and can thus be used in conjunction with the Goose Bay and Cartwright data to develop a long-running climate record for the Mealy Mountains. Data were interpolated at both local climate stations (570 m and 1000 m), allowing for the calculation of adiabatic rates.

3.2.3 Climate data interpolation

To interpolate a long-running series of climate data for the Mealy Mountains, an ordinary least-squares (OLS) regression was performed using climate data from Goose Bay and Cartwright (Hanson, 1987). The maximum daily temperature data for all years was compiled by month into separate files. Maximum temperatures are used in this study because they represent the upper limit of vegetation growth (Miller, 2005). Additionally,

33

the mean temperatures for the Cartwright and Goose Bay weather stations are an average of the minimum and maximum values for each day and not a running average of all values collected. OLS regressions were performed using the Cartwright and Goose Bay data as the independent variables against the upper (1000 m) and lower (570 m) elevation Mealy Mountain climate stations. The resulting coefficients and constants were used to interpolate the Mealy Mountains climate data to cover the entire time frame of interest. The interpolated results were compared to the observed climate data from the Mealy Mountains climate stations.

The calculated regression coefficients and constants are based on daily data, grouped into separate monthly files. Therefore, these coefficients represent average monthly conditions. While the input data contained daily values, the interpolated results will be monthly averages.

The seasonal fluctuations in coefficients suggest a greater influence from Maritime weather patterns, represented by the Cartwright climate data, during the winter months. In the summer months, the Mealy Mountains are more influenced by inland, continental weather patterns, as represented by the Goose Bay climate data (Figure 3.5). Table 3.2 lists the monthly coefficients and constants for the upper and lower climate stations.

The Root Mean Square Error (RMSE) was calculated between the observed and predicted temperatures for the upper and lower climate stations. The RMSE for the upper climate station is 0.777° C. The RMSE for the lower climate station is 0.969° C. These

34

error values prove the efficacy of the OLS regression model for predicting long term

temperature values for the Mealy Mountains.

Table 3.2 Upper and lower climate station regression coefficients for maximum
temperature

	Lower Climate Station			Upper Climate Station		
	Cartwright	Goose Bay	Constant	Cartwright	Goose Bay	Constant
January	0.628	0.243	-3.332	0.452	0.347	-5.822
February	0.949	0.250	1.227	0.632	0.282	-5.705
March	0.688	0.330	-1.954	0.866	0.169	-5.805
April	0.378	0.465	-1.519	0.562	0.363	-6.006
May	0.300	0.581	-2.138	0.275	0.559	-5.913
June	0.230	0.562	0.255	0.246	0.585	-4.891
July	0.193	0.623	0.378	0.252	0.482	-0.965
August	0.237	0.624	-0.330	0.205	0.600	-3.505
September	0.385	0.586	-2.965	0.450	0.519	-7.189
October	0.656	0.390	-4.085	0.563	0.425	-6.977
November	0.671	0.350	-3.578	0.646	0.422	-6.364
December	0.716	0.296	-2.753	0.706	0.280	-5.675
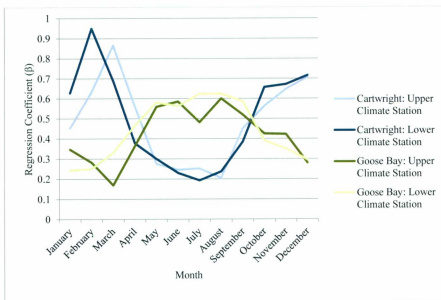
Figure 3.5 Upper and lower climate station regression coefficients for maximum temperature

3.2.4 Adiabatic rates

Adiabatic rates were calculated using the averaged maximum temperatures for June to September for years corresponding to the satellite imagery (1983, 2001, 2005, and 2008).

The rate of change values are calculated by dividing the difference between the upper and lower climate stations by the elevation difference between the two stations (Equation 3.1).

$$AR_{year} = \frac{T_u - T_l}{E_u - E_l}$$

Equation 3.1 Adiabatic rate

Where:
AR_{year} = adiabatic rate for year of interest;
T_u = upper climate station temperature;
T_l = lower climate station temperature;
E_u = upper climate station elevation;
E_l = lower climate station elevation.

The adiabatic rates were developed using map algebra calculations. The DEM for the study area was rescaled using raster algebra such that elevations of 570 m became zero. Elevations higher than 570 m became increasingly negative, while elevations lower than 570 m became increasingly positive. If a temperature is known at 570 m, it is expected that at lower elevations the temperature is higher and at higher elevations it is lower. Next, the following algebra was applied to the above mentioned raster layer:

$$Adiabatic\ Layer = T_{year} + AR_{year}(Rscl\_Elev)$$

Equation 3.2 Raster algebra performed to develop adiabatic change layers

Where:
Adiabatic Layer = the output adiabatic layer for the study area;
T_{year} = average J-J-A-S maximum temperature for each year;
AR_{year} = the known adiabatic rate for each given year;
Rscl_Elev = the rescaled elevation layer (where 570 m is equal to 0).

The output of this operation is a separate layer for each year in which higher elevations have lower temperatures and vice versa. At elevations of 570 m and 1000 m, the temperatures on the adiabatic layers correspond to that of the lower and upper climate stations, respectively. An example of an adiabatic rate layer for 2008 is shown in Figure 3.6.
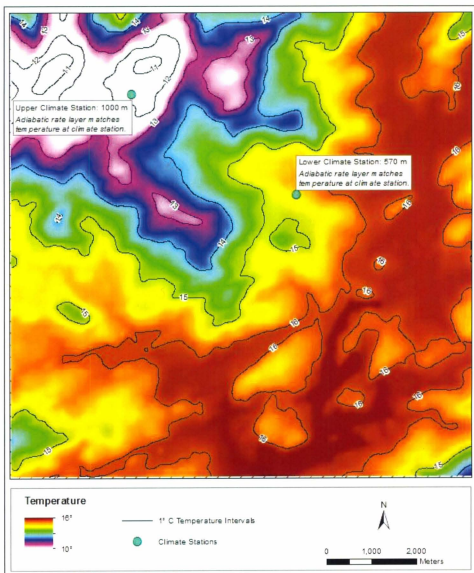
Figure 3.6 Adiabatic rate layer for 2008, showing 1° C temperature intervals and upper and lower climate station

Table 3.3 lists the averaged maximum temperatures for June to September from 1983 to 2008 for both climate stations, as well as the calculated rate of change values for each year.

Table 3.3 Rate of change in temperature (June to September maxima; imagery years shown in bold)

Year	Lower Climate Station (°C)	Upper Climate Station (°C)	Rate of Change (°C/m)
1983	**14.2**	**10.1**	**-0.0095**
1984	14.0	9.8	-0.0097
1985	13.7	9.6	-0.0095
1986	13.0	8.9	-0.0095
1987	13.9	9.8	-0.0095
1988	13.9	9.7	-0.0096
1989	14.3	10.3	-0.0094
1990	13.7	9.7	-0.0094
1991	12.9	8.8	-0.0096
1992	13.5	9.5	-0.0094
1993	13.7	9.6	-0.0096
1994	14.2	10.1	-0.0095
1995	14.6	10.5	-0.0096
1996	14.1	10.0	-0.0095
1997	13.7	9.7	-0.0093
1998	14.5	10.4	-0.0095
1999	15.4	11.4	-0.0095
2000	15.2	11.1	-0.0096
2001	**14.3**	**10.3**	**-0.0094**
2002	14.4	10.3	-0.0094
2003	16.1	12.0	-0.0095
2004	14.8	10.6	-0.0097
2005	**15.3**	**11.2**	**-0.0096**
2006	15.9	11.9	-0.0094
2007	15.0	10.9	-0.0096
2008	**15.5**	**11.3**	**-0.0097**

3.3 Aerial photography and satellite imagery

Aerial photography (from 1950) and satellite imagery (spanning from 1983 to 2008) were collected for the study area. The satellite images were collected between late July and mid-September. Satellite image resolution varied from 15 m to 79 m. All of the images, with the exception of the aerial photographs, capture data in the visible and near-infrared wavelengths. Table 3.4 lists the types of imagery and spatial resolutions.

Table 3.4 Details of aerial photography and satellite imagery

Date	Sensor and Platform	Resolution (m)	Band Configuration	Re-sampling RMS (m)
1950	Airborne	~1.3	N/A	N/A
24 July1983	Landsat 4 MSS	79	B, G, R, NIR	35.9
20 September 2001	Landsat 7 ETM+	30	B, G, R, NIR, TIR	Used as base image
6 September 2005	Quickbird	2.5	B, G, R, NIR	Image not re-sampled
13 September 2005	ASTER - TERRA	15	3 bands from 0.52-0.86 μm	50.1
30 August 2008	SPOT 4 - HRVIR	20	G, R, NIR	12.9

Eight aerial photographs from 1950 were used to cover the study area. To account for photo distortions due to elevation, the images were scanned and orthorectified. They were then mosaicked and cropped to form a single, continuous image spanning a region larger than that of the study area. The aerial photographs were not used in the change detection methods. However, they were used to delineate an approximate boundary between forested and non-forested areas. The delineation was used as a binary (forest vs. non-forest) variable within the Bayesian probability layers, as discussed later.

40

All satellite imagery was georeferenced and resampled to 20 m resolution. This resolution represented the only option with regards to resampling given the original resolution of the images (Table 3.4). Radiometric and atmospheric corrections were also performed to minimize differences between images due to fluctuations in atmospheric conditions at the time of image acquisition. The details of the corrections performed are given in Appendix B. Multi-temporal imagery has the potential provide insight into the degree of change that has occurred over the past 25 years. The procedure and specifics of the above mentioned corrections are outlined in Appendix B.

To facilitate change detection and modelling efforts, the images were classified using a supervised classification algorithm. This procedure delineates land covers based on training sites provided by the user. This method tends to produce higher classification accuracies with more modifiable training and testing sites (Eastman, 2009).

The satellite images were classified using a combination of field data and user knowledge, in conjunction with a high-resolution Quickbird image from 2005. The field data are used to develop training sites where a dominant land cover is identifiable. In areas with sparse field data coverage, a combination of user knowledge from field surveys and high resolution Quickbird imagery was used to delineate homogenous land cover types. This ancillary data was most useful for the coniferous shrub (CSH) and bedrock/exposed (BRK) land cover classes, as these areas are easily distinguishable on the Quickbird image. Training sites were delineated on the 2008 image, as this was the same year the field data were collected. Therefore, it is logical to assume that in earlier images the land covers were not exactly the same. If there was a change in the land cover

from earlier dates to 2008, the classification accuracies may be lower. Table 3.5 lists the classification accuracies for each image. Note that the 'no data' and water areas have been removed from the overall accuracy calculations

Table 3.5 Satellite image classification accuracies derived from Kappa coefficient of agreement

	2008	2005	2001	1983
	SPOT	ASTER	LETM+	LMSS
DSH	0.5957 (60%)	0.6608 (66%)	0.8239 (82%)	0.6860 (69%)
CSH	1.0000 (100%)	0.8869 (89%)	1.0000 (100%)	0.8618 (86%)
HTH	0.5824 (58%)	0.5833 (58%)	0.5351 (53%)	0.3684 (37%)
BRK	0.5625 (56%)	0.8747 (87%)	0.6630 (66%)	0.3568 (36%)
Overall	0.6363 (63%)	0.7345 (73%)	0.7148 (71%)	0.5163 (52%)

Figures 3.7 to 3.10 presents the final classified images. The line marking the approximate transition between forested and non-forested areas, as delineated from the aerial photographs, is displayed.

3.4 Topographic data

Topographic data, including elevation, slope, aspect, exposure, topographic relative moisture index (TRMI), and topographic shape index (TSI), were extracted from a 1:50,000 scale digital elevation model (DEM). These data were used in conjunction with the aerial and satellite imagery to determine the effect that topographic conditions have on vegetation change.

Elevation and slope are measurements extracted from DEMs in most spatial analysis software and are not discussed here. The remaining indices, however, required further processing.
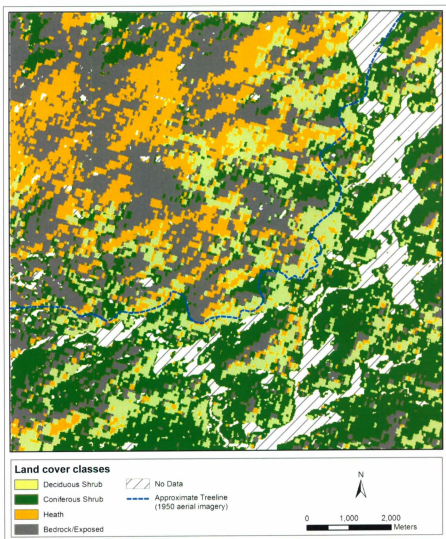
Figure 3.7 Land cover classification (1983)

Land cover classes

Deciduous Shrub
Coniferous Shrub
Heath
Bedrock/Exposed

No Data
Approximate Treeline
(1950 aerial imagery)

N

0 1,000 2,000
Meters

Land cover classes

- Deciduous Shrub
- Coniferous Shrub
- Heath
- Bedrock/Exposed
- No Data
- Approximate Treeline (1950 aerial imagery)

N

0   1,000   2,000
Meters
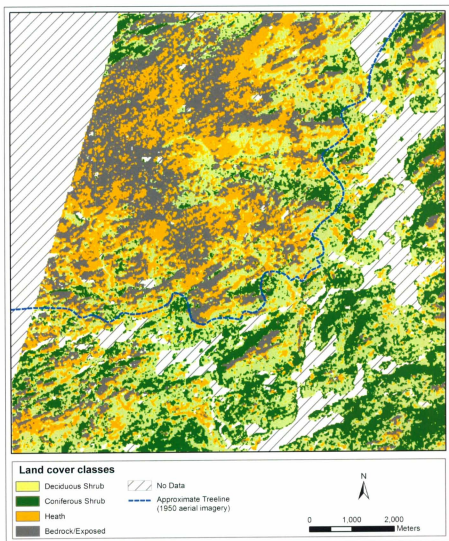
Figure 3.8 Land cover classification (2001)
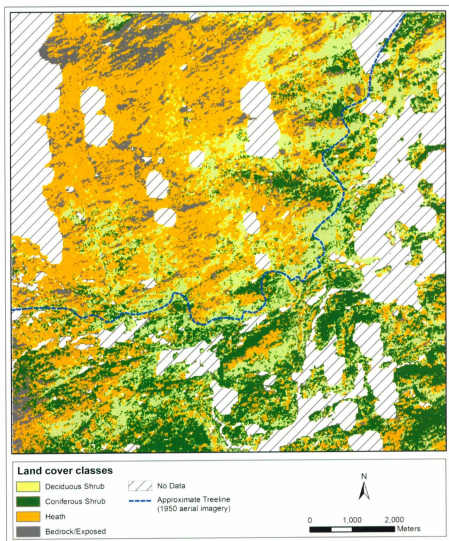
Figure 3.9 Land cover classification (2005)

Land cover classes

Deciduous Shrub		No Data	
Coniferous Shrub		Approximate Treeline (1950 aerial imagery)	
Heath			
Bedrock/Exposed			

N

0   1,000   2,000
Meters
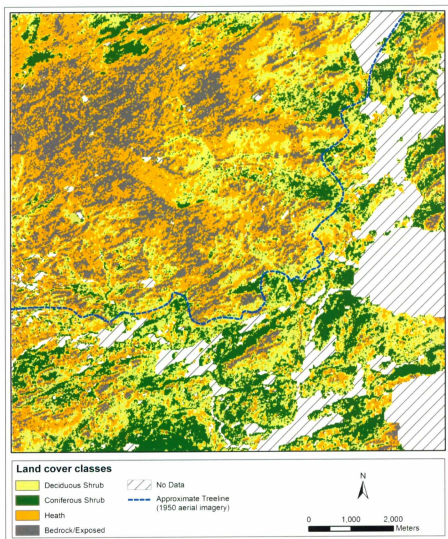
Figure 3.10 Land cover classification (2008)

46

Due to the circular nature of aspect, problems can arise when attempting to determine its effect on vegetation patterns. Miller (2005) proposes a "southwestness" (SWness) index. Miller's index, however, is given for degrees (°), when it should be calculated with radians, as the original formula produced output errors. The adaptation of Miller's (2005) equation, with degrees converted to radians, is:

$$SWness = \cos(asp) - \cos(rad(225°))$$

Equation 3.3 Modified southwestness (SWness) index

Where:
$SWness$ = the modified southwestness index (ranging from -1.0 to 1.0);
asp = the original aspect layer in radians;

The topographic shape index (TSI), adopted from McNab (1989), is a measure of the shape and position of the land as it relates to the land forms surrounding it. For example, valley floors tend to have highly negative values, valley walls have TSI values approaching 0, and mountain peaks and ridges have highly positive TSI values. Areas with highly variable elevations tend to have a broader TSI range. Regions such as the Mealy Mountains, characterised by rolling hills and gentle slopes, tend to have a more constrained TSI range. The TSI, calculated using map algebra, is as follows:

$$TSI = DEM - focalmean(dem, neighbourhood, x)$$

Equation 3.4 Topographic shape index (TSI)

Where:
TSI   = topographic shape index;
DEM   = the digital elevation model for the area;

neighbourhood = the shape of the neighbourhood surrounding the pixel of interest (*e.g.* circle, square, etc.);
x   = the distance of the search neighbourhood in pixels.

The topographic relative moisture index (TRMI), developed by Parker (1982), is a measure of the soil moisture potential of an area. It should be noted that this index measures potential only, and thus has no way of incorporating seasonal fluctuations of water content. The TRMI, ranging from 0 to 60, is calculated by rescaling topographic positions (from the TSI), slope configuration (curvature), slope steepness (slope in degrees), and slope aspects (in degrees azimuth) into discrete classes and summing the result. Areas with low values tend to exhibit drier conditions while higher values tend to be much wetter.

The angle to sheltering topography, herein referred to as exposure, was adapted from Harrison and Kelly (1996). A number of hillshades were calculated with incrementally decreasing sun altitudes ranging from 85° to 15° in an attempt to mimic wind (*i.e.* wind does not originate at a single point source). The shaded areas were taken from each hillshade and coded as 1, whereas areas not shaded were coded as 0. This was performed for each different sun altitude with the results summed. Higher values in the resultant layer indicated more sheltered areas. This process was completed three times: once for the dominant wind direction (22.5°), and once each for 20° north (2.5°) and south (42.5°) of the dominant wind direction. The three resulting layers were then

combined using a weighted average where the dominant wind direction was given the highest weight (50%) (Harrison and Kelly, 1996).

3.5 Bayesian probabilities

A conditional Bayesian probability is calculated by adding predictive variables to a prior probability, thus creating a posterior probability. A prior probability, for example, is the probability of finding deciduous shrub within a study area, while only considering the proportion of the study area occupied by deciduous shrub (Equation 3.5).

$$P\{DSH\} = \frac{N\{DSH\}}{N\{Total\}}$$

Equation 3.5 Prior probability

Where:
$P\{DSH\}$ = prior probability of finding, in this case, deciduous shrub
$N\{DSH\}$ = total number of deciduous shrub cells (or the total area of deciduous shrub)
$N\{Total\}$ = total number of cells in the study area (or the total area).

For example, the posterior probability is calculated when one assumes that deciduous shrub occurs on south-facing slopes. This knowledge is added to the prior probability (Equation 3.6). Any number of predictive variables or conditions can be added to the prior probability.

$$P\{DSH|ASP_S\} = \frac{P\{DSH \cap ASP_S\}}{P\{ASP_S\}}$$

Equation 3.6 Example of posterior probability

49

Where:

$P\{DSH|ASP_S\}$ = posterior probability of finding deciduous shrub given a south-facing aspect

$P\{DSH \cap ASP_S\}$ = $N\{DSH|ASP_S\} / N\{Total\}$ = probability of deciduous shrub and south-facing slopes both occurring

$P\{ASP_S\}$ = $N\{ASP_S\} / N\{Total\}$ = probability of south-facing slopes

(adapted from Bonham-Carter, 1994).

Bayesian probability layers were created to demonstrate the propensity for a particular land cover to be present within the study area given specified topographic conditions. To develop the probability layers, each of the topographic and adiabatic layers were rescaled into discrete classes (Table 3.6).

Table 3.6 Reclassification of Bayesian probability input layers

Layer	Interval	Number of Classes	Classification Scheme
Elevation	50 m	13	Range: ~475-1100
Exposure	0.25	5	0-0.25; 0.25-0.5; 0.5-0.75; 0.75-1
Slope	N/A	7	0-2%; 2-5%; 5-8%; 8-15%; 15-30%; 30-60%; >60%
Aspect	45	8	N: 337.5-0-22.5°; NE: 22.5-67.5°; E: 67.5-112.5°; SE: 112.5-157.5°; S: 157.5-202.5°; SW: 202.5-247.5°; W: 247.5-292.5°; NW: 292.5-337.5°

Table 3.6 cont'd

Layer	Interval	Number of Classes	Classification Scheme
TSI	N/A	4	1: 150 - 1100 (ridge); 2: -100 - 150 (slope); 3: -200 - -100 (toe slope); 4: -1100 - -200 (valley bottom)
TRMI	10	5	Range: 14-52
Adiabatic	1° C	8	Range: −9-16° C

Only a portion of the classification schemes for the topographic variables are referenced in the literature. A correlation analysis was performed to determine if there existed any trends between the land cover classes and elevation. However, there were no discernable trends present. Thus, elevation was divided into 12 discrete, 50 m classes. Exposure was divided into 5 classes. Slope was divided based on the convention of the European Commission (2010). Aspect was divided into the cardinal (N, E, S, W) and inter-cardinal (NE, SE, SW, NW) directions. The TSI layer was classified based on Zimmerman's (2000) method, whereby valleys, lower and upper slopes, and ridges are identified. The TRMI layer was divided into 5 equal interval classes. Finally, the adiabatic layers were divided into 1° C intervals. The vegetation land cover classes (not listed in Table 3.6) maintained the same, discrete classes as before (deciduous shrub, coniferous shrub, heath, bedrock/exposed).

Once classified, all of the layers listed in Table 3.6 are overlayed. The result is a single layer with polygons that represent unique conditions. Each discrete polygon in this layer is some combination of the above mentioned topographic layers. This procedure is performed again, but this time, the land cover classifications are included as well. This produces another layer with even more unique conditions. Next, the area of each unique-condition polygon is calculated for both layers. This area value is divided by the total study area size, thus giving probabilities of occurrence. Subsequently, all of the polygons with the same set of unique conditions were dissolved to form a single, multi-part polygon. The probability field of the individual polygons was summed, based on the additive property of probabilities (McClave and Sinich, 2000). The result was a layer with fewer unique-condition polygons and a probability value that was higher than the original for each polygon. Using the unique-condition layer that includes the land cover classifications, each land cover class was selected and extracted to its own layer. The result was four new unique-condition layers (one for each of the four land cover classes). These four layers were divided (using map algebra) by a raster of the topographic variables unique-condition layer (Figure 3.11). In order to incorporate the satellite image classification accuracies, each of the Bayesian probabilities were multiplied by the classification accuracy for a particular land cover within a particular year (*e.g.* the 2005 Bayesian probability for coniferous shrub was multiplied by 0.8869. This value represents the classification accuracy of coniferous shrub in the 2005 image, as listed in Table 3.5)

The final output contained 16 separate layers: four layers for each of the land covers within each of the four years. Figure 3.12 shows an example of one of the Bayesian probability layers for coniferous shrub in 2008. Note that the extent of the probabilities is restricted to that of the coniferous shrub for 2008. Outside of the coniferous shrub area, the probability of finding coniferous shrub declines to 0.
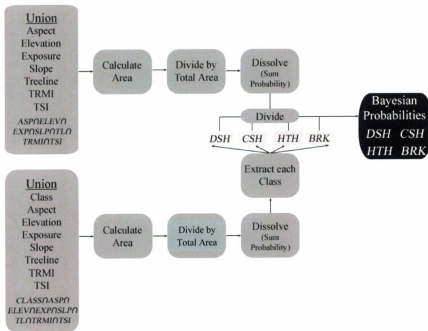
Figure 3.11 Procedure for developing Bayesian probabilities for each image year
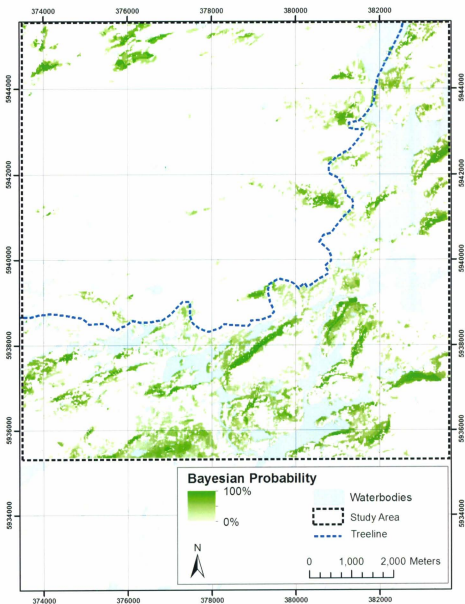
Figure 3.12 Sample Bayesian probability for coniferous shrub (2008)

3.6 Summary

This chapter provided details on the processing of the data necessary for the detection of land cover and climate changes. The processing steps were as follows:

- Analysis of field data;
- Regional and local climate data analysis and interpolation;
- Calculation of adiabatic rates;
- Preparation of aerial photography and satellite imagery;
- Preparation of topographic variables;
- Calculation of Bayesian probabilities.

The outputs from these processing steps will be used for exploratory analysis, which in turn will develop the input parameters for the cellular automata-Markov chain model.

4. EXPLORATORY ANALYSIS

Relationships between topographic variables and land cover classes must be explored to facilitate model development. This permits one to determine the best suited predictor variables to use with the model, as well as discover how certain variables influence vegetation patterns. Section 4.1 describes the variability of land covers amongst topographic variables. Section 4.2 discusses the the yearly changes in land cover, the yearly changes in land covers as they relate to topographic variables, and changes in Bayesian probability.

4.1 Variability of land covers amongst topographic variables

This section discusses how the land cover classes are distributed with regards to certain topographic conditions. Aspect, elevation, and topographic shape index (TSI) are analysed. The remaining variables (exposure, slope, treeline position, and TRMI), while not thoroughly discussed here, were still included in the CA-Markov model because of their added predictive power to the cellular automata. Chapter 5 discusses a model validation procedure whereby a CA-Markov model was developed using only aspect, elevation and TSI as inputs.

The purpose of this analysis is to determine if particular land cover classes favour certain topographic conditions. It is expected that less resilient vegetation, such as deciduous shrubs, will favour less-exposed slopes. Coniferous shrubs will likely be situated on more exposed slopes. At high elevations, heath is expected to be dominant.

Holland and Steyn (1975) and Miller (2005) highlight the importance of aspect in the growth and movement of vegetation upslope. Polar graphs plot the distribution of

56

aspect within each land cover class (Figures 4.1 to 4.4). Examination of these graphs indicates that coniferous shrub is dominant on north- and northwest-facing slopes. For the 1983 and 2001 images, heath is most evident on southeast-facing slopes, but in 2005 and 2008, it appears to be more widespread, though still predominantly in the southeast-facing direction. Deciduous shrub appears predominantly towards the southeast-facing slopes. Table 4.1 lists the dominant aspects for each of the four land cover classes.

Table 4.1 Dominant aspects for each land cover class

Land Cover Class	Dominant Aspect
DSH	90-180° (SE)
CSH	275-50° (NW, N)
HTH	95-190° (SE)
BRK	0-90° (NE), 180-260° (SW)
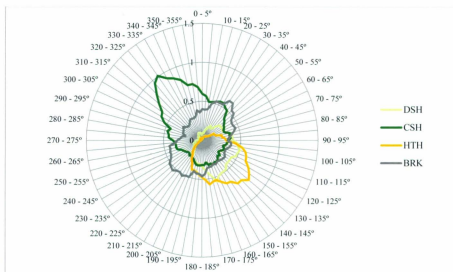
Figure 4.1 Distribution of aspect by land cover class (1983) (in km^2)
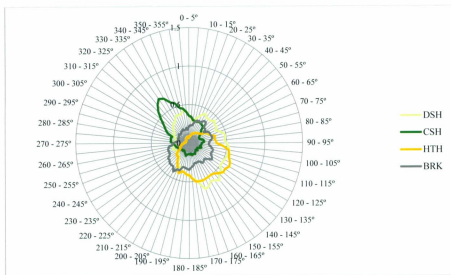
Figure 4.2 Distribution of aspect by land cover class (2001) (in km^2)
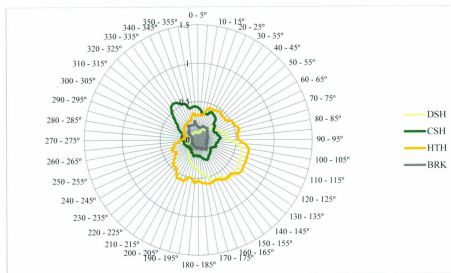
Figure 4.3 Distribution of aspect by land cover class (2005) (in km^2)
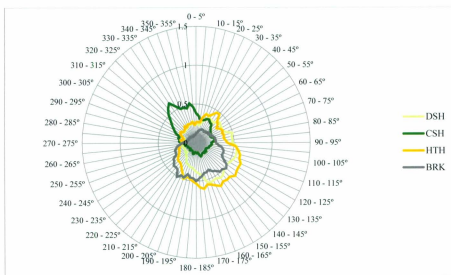
Figure 4.4 Distribution of aspect by land cover class (2008) (in km^2)

Figures 4.5 to 4.8 present the distribution of the land cover classes by elevation.

The Elevation - % Cover Index (ECI) was calculated by multiplying the percentage cover

of a particular land cover at a particular elevation range by the percent of land at that

elevation range, relative to the entire study area (Equation 4.1)

$$ECI = LC_{ax} * L_x$$

Equation 4.1 Elevation - % land cover index

Where:
LC$_{ax}$ = Percentage of land cover a at elevation range x
L$_x$ = Percentage of land at elevation range x (in relation to total study area)

The purpose of this index is to differentiate elevation ranges with greater land area

(low to mid-elevations) from those with lesser land area (higher elevations). Due to

terrain shape, there is more land area at lower elevations, and less at higher elevations. The majority of the land area is situated between 475 m and 700 m.

Figures 4.5 to 4.8 indicate that deciduous and coniferous shrubs tend to occupy a greater percentage of the land at lower elevations. As deciduous and coniferous shrubs decline with increasing elevation, heath and bedrock/exposed land covers begin to dominate in total area occupied. Above approximately 750 m, deciduous and coniferous shrubs occupy less than 20% of the landscape. This is evidence that higher elevations are less hospitable to deciduous and coniferous shrub. Thus, it is unlikely there will be growth of shrubs in these locations.
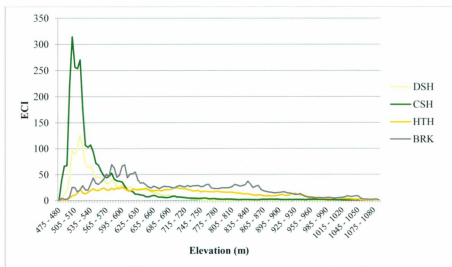
Figure 4.5 ECI by elevation range for each land cover class (1983)
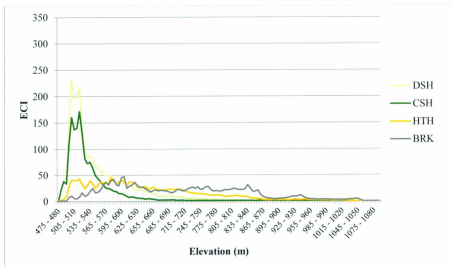
Figure 4.6 ECI by elevation range for each land cover class (2001)
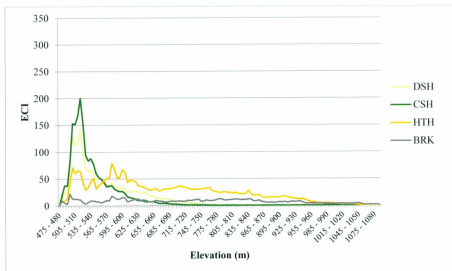
Figure 4.7 ECI by elevation range for each land cover class (2005)
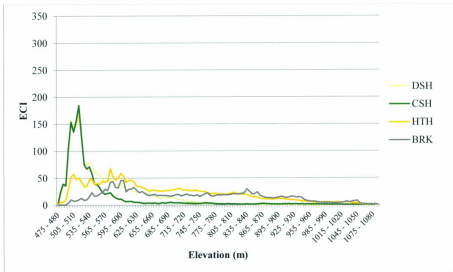
Figure 4.8 ECI by elevation range for each land cover class (2008)

The topographic shape index (TSI) graphs demonstrate how land cover types vary with change in topographic position. The TSI ranges from approximately -150 (valley floors) to 185 (ridges). Figures 4.9 to 4.12 show the TSI - % cover index (TCI) (calculated as in Equation 4.1, but with TSI substituted for elevation) in relation to the TSI range. The purpose of this index is to differentiate between the total land area across different terrain characteristics (*e.g.* mid-slopes, valley floors, ridges, etc.)
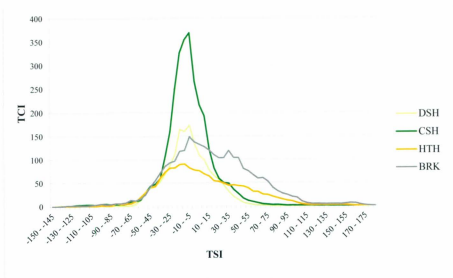
Figure 4.9 TCI by TSI range for each land cover class (1983)
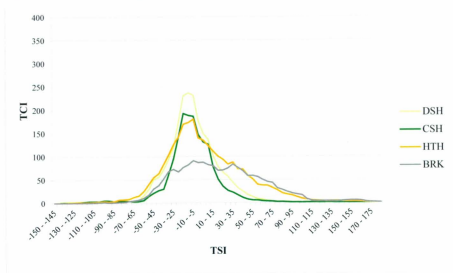
Figure 4.10 TCI by TSI range for each land cover class (2001)
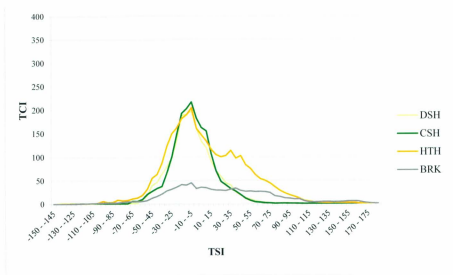
Figure 4.11 TCI by TSI range for each land cover class (2005)
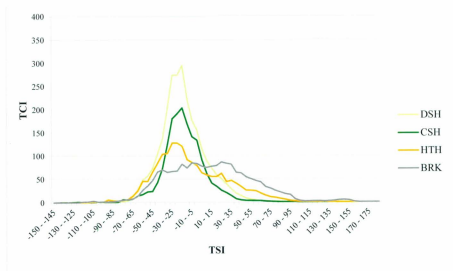
Figure 4.12 TCI by TSI range for each land cover class (2008)

Figures 4.9 to 4.12 reveal that most of the land area exists between -60 and 100 on the TSI scale. The majority of the deciduous and coniferous shrubs reside on the valley floors and toe slopes (-150 - ~0) and continuing slightly farther upslope. Beyond a TSI value of 50, there is an insignificant amount of either deciduous or coniferous shrub; this value does not change over time. Heath and bedrock/exposed land covers continue to be present towards upper slopes and ridge tops, where conditions are more exposed. This suggests that the more exposed areas tend to be less favourable to deciduous and coniferous shrub, thus heath and bedrock/exposed are dominant.

4.2 Change detection

This section outlines the change in topographic variables and Bayesian probabilities within each land cover class from year to year. This analysis will determine if vegetation experienced infilling of movement in certain areas.

4.2.1 Change in land cover from 1983 to 2008

Table 4.2 lists the total area (in square kilometres and as a percentage) of each land cover class from 1983 to 2008. The no-data regions have been excluded from the calculations.

Table 4.2 Total area (km^2) of each land cover class

	1983	2001	2005	2008
DSH	17.3 (18.3%)	27.3 (32.7%)	19.9 (24.2%)	24.1 (26.8%)
CSH	31.4 (33.3%)	17.8 (21.3%)	20.5 (25.0%)	17.8 (19.8%)
HTH	16.9 (17.9%)	18.6 (22.3%)	32.0 (39.0%)	27.9 (31.1%)
BRK	28.6 (30.4%)	19.7 (23.6%)	9.7 (11.8%)	20.0 (22.2%)

There is considerable fluctuation in the area of each land cover from 1983 to 2008 (Figure 4.13). Deciduous shrub alternates between gains and losses, while coniferous shrub fell drastically from 1983 to 2001, with a slight increase to 2005, followed by another decrease to 2008. Heath increased from 1983 to 2005, but then decreased to 2008. Bedrock/exposed regions decreased steadily from 1983 to 2005, but increased again in 2008. The most likely explanation for these fluctuations is attributed to the patchy nature of heath. Heath and bedrock tend to occupy the same topographic conditions; however, there are rarely vast expanses of either of the land covers. Rather, they occur in small, disjointed patches. Their patchy nature, whereby heath is interspersed with bedrock/exposed, leads to mixed spectral signatures between the two classes. This explains the variations in heath and bedrock/exposed from 2005 to 2008.
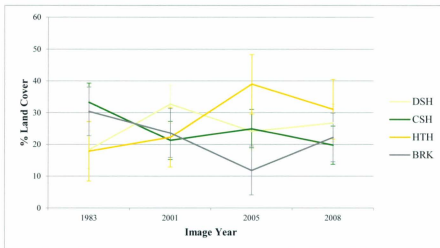
Figure 4.13 Percent area for each land cover class (1983-2008) with standard deviation

4.2.2 Variability of topographic variables between years

The change in topographic conditions for each of the land cover classes are investigated in this section. The purpose of this analysis is to determine if vegetation is migrating to new topographic positions (*e.g.* more exposed aspects, higher elevations, etc.).

Figures 4.14 to 4.17 present polar plots of the year-to-year variation in aspect as defined by each of the four land cover classes. The purpose of this analysis is to determine if the land covers migrated to different aspects. Deciduous shrub does not appear to have migrated to any different aspects (Figure 4.14). In 2001, there were instances on north-facing slopes, but the majority of deciduous shrub is located on southeast-facing slopes. Coniferous shrub remained stationary from 1983 to 2008 (Figure 4.15). Heath remained on southeast-facing slopes through all years of the analysis as well (Figure 4.16).
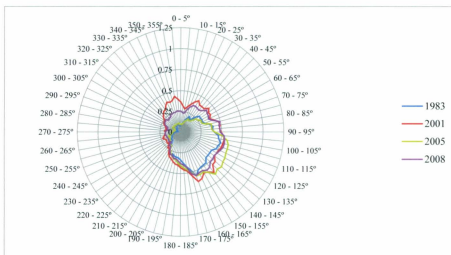
Figure 4.14 Aspect of deciduous shrub (1983-2008) (in km2)
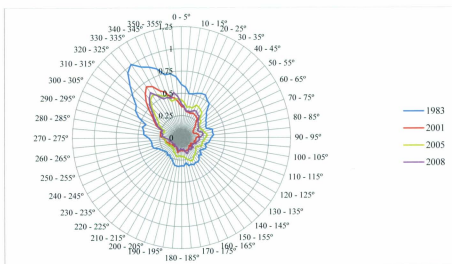
Figure 4.15 Aspect of coniferous shrub (1983-2008) (in km^2)
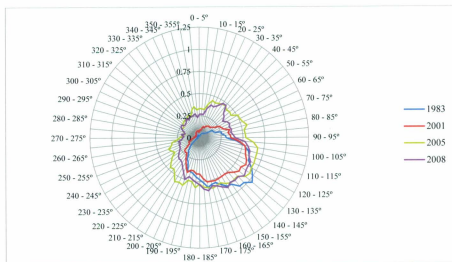
Figure 4.16 Aspect of heath (1983-2008) (in km^2)
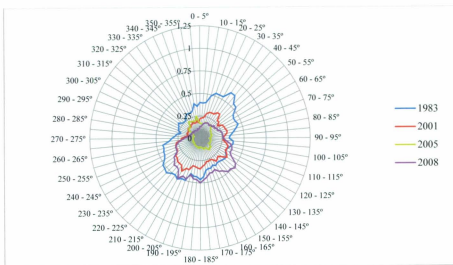
Figure 4.17 Aspect of bedrock/exposed (1983-2008) (in km^2)

Bedrock/exposed became more restricted to southeast- and southwest-facing slopes beyond 1983 (Figure 4.17). However, the observed changes in bedrock/exposed are likely due to pixel-mixing between bedrock/exposed and heath.

Figures 4.18 to 4.21 present year-to-year variation in elevation for each of the four land cover classes. The most evident change observed is with the heath class (Figure 4.20). There was an increase in the percentage of land occupied by heath from 1983 to 2005, with a small decrease to 2008.

Deciduous and coniferous shrubs changed less from year to year. The percentage of deciduous shrub (Figure 4.18) increased from 1983 to 2001, decreased in 2005, before rising again in 2008. Coniferous shrubs decrease from 1983 to 2001, after which there was little change. With the exception of 2008, the bedrock/exposed land cover (Figure

4.21) decreased steadily, suggesting an increase in heath, or pixel-mixing between the two classes. These changes are consistent with those seen in Table 4.2 and Figure 4.13.

While the variability of these data are high, it does not suggest changes did not occur. Given that most vegetation shifts occur over decadal time scales, large changes will generally not be evident from 2001 to 2008 (Pereg and Payette, 1998; Epstein *et al.*, 2004; Stow *et al.*, 2004; IPCC, 2007).
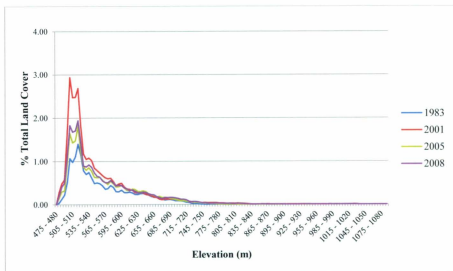
Figure 4.18 Elevation of deciduous shrub (1983-2008)
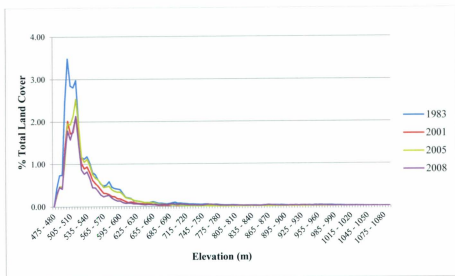
Figure 4.19 Elevation of coniferous shrub (1983-2008)
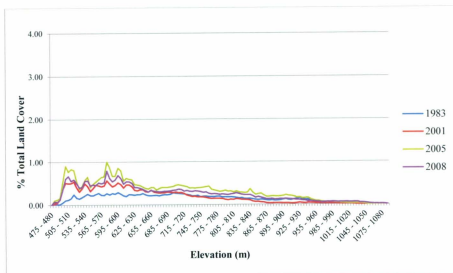
Figure 4.20 Elevation of heath (1983-2008)
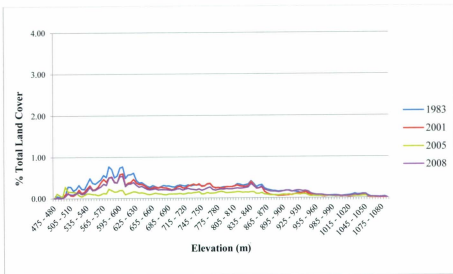
Figure 4.21 Elevation of bedrock/exposed (1983-2008)

4.2.3 Percent change in Bayesian probabilities

The percentage change in deciduous and coniferous shrub was calculated between 1983 and 2008 (Figures 4.22 and 4.23, respectively). The topographic shape index is shown below the percent change layer to provide a general characterization of the topography in high change areas. Deciduous shrub (Figure 4.22) decreased from 1983 to 2008 over a great deal of the lower elevations. South-facing slopes (where deciduous shrub is frequently found) witnessed small increases. Most notable, however, was the movement of deciduous shrub along valley floors (TSI range: ~-150 - ~0) from lower to higher elevations. Coniferous shrubs (Figure 4.23) increased in the lower elevations, with minimal increases along the valley floors. North-facing slopes (where coniferous shrub is prominent) witnessed increases as well.
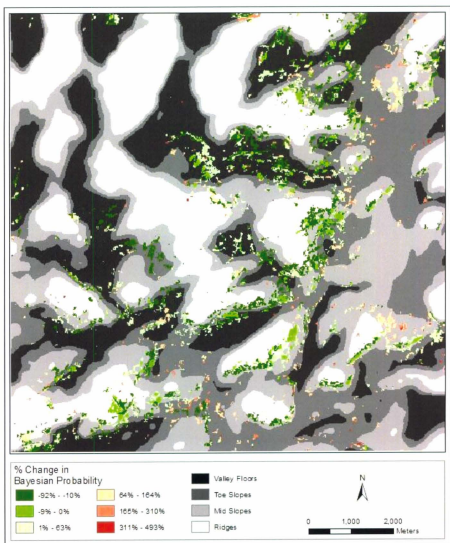
Figure 4.22 Percentage change in Bayesian probabilities for deciduous shrub (1983-2008)

% Change in Bayesian Probability

- -96% - -40%
- -39% - -12%
- -11% - 0%
- 1% - 38%
- 39% - 122%
- 123% - 290%

Valley Floors
Toe Slopes
Mid Slopes
Ridges

N

0   1,000   2,000 Meters
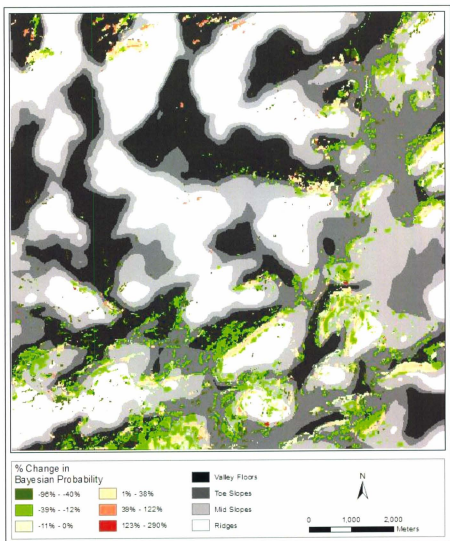
Figure 4.23 Percentage change in Bayesian probabilities for coniferous shrub (1983-2008)

Figures 4.24 and 4.25 present the relationship between aspect and Bayesian probability for deciduous (Figure 4.24) and coniferous (Figure 4.25) shrub. The Bayesian probability for deciduous shrub doubled (from 0.19 to 0.38) in the west-facing directions (270°). All other changes were considerably less than this; however, there were substantial changes in the southwest and northeast-facing directions as well.

The Bayesian probability for coniferous shrub increased considerably in all but the southeast-facing direction. Most notable is the 279% increase (from 0.17 to 0.65) in the northwest-facing direction. There were also increases in the west- and north-facing directions.
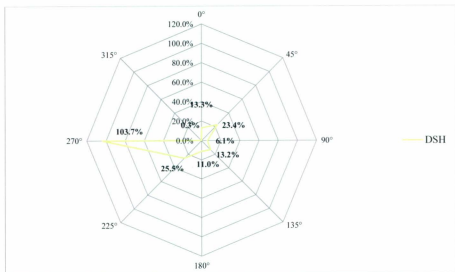
Figure 4.24 Relationship between percent change in Bayesian probability and aspect for deciduous shrub (1983-2008)
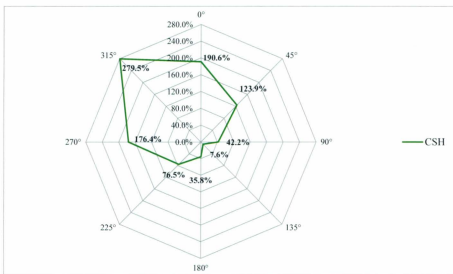
Figure 4.25 Relationship percent change in Bayesian probability and aspect for coniferous shrub (1983-2008)

Figures 4.26 and 4.27 relate changes in Bayesian probability to elevation for deciduous shrub (Figure 4.26) and coniferous shrub (Figure 4.27). The average Bayesian probability for deciduous shrub increased from 1983 to 2008 over all elevation ranges. Considering that deciduous shrub tends to be located at lower elevations, the approximately 100% increase in the 450-500 m range is important. Lesser changes occur at higher elevations. Above 700 m, there appear to be large changes; however, because there is little deciduous shrub at higher elevations, a small increase could result in a doubling or tripling of total area. All of the above noted changes exhibit high standard deviations, thus making these changes insignificant. This does not mean, however, that

changes did not occur. Rather, the variability of the changes across particular elevation ranges is very high.

Coniferous shrub (Figure 4.27) exhibited smaller changes in the lower elevations, but higher changes around the 700-900 m elevation range. However, the same issue exists here as with deciduous shrub. The standard deviations for the change values are all extremely high. Again, this does not indicate that change didn't occur, just that the variability of change within each elevation range was high.
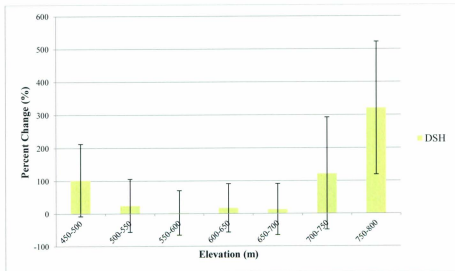
Figure 4.26 Relationship between percent change in Bayesian probability and elevation for deciduous shrub (1983-2008)
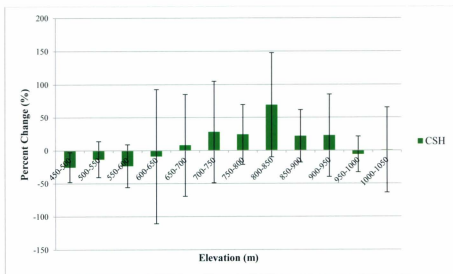
Figure 4.27 Relationship between percent change in Bayesian probability and elevation for coniferous shrub (1983-2008)

The relationship between percent change in Bayesian probability and topographic shape index is presented in Figure 4.28 (deciduous shrub) and 4.29 (coniferous shrub). The highest change in deciduous shrub occurred in the toe slopes (TSI range: -100-0) and mid-slopes (TSI range: 0-100), where Bayesian probabilities increased by about 20% each. Change in the valley floors (TSI range: -147--100) and along ridges (TSI range: 100-180) were negligibly or non-existent. The data presented here exhibits very high standard deviations, suggesting the data are insignificant. Again, this does not suggest that change did not occur. It is an indication that variability within each TSI range was high.

Coniferous shrub (Figure 4.28) increased by approximately 40% in the valley floors (TSI range: -147--100). Along the toe slopes (TSI range: -100-0) and mid-slopes (TSI range: 0-100), Bayesian probabilities decreased by less than 20%. There was a small increase in Bayesian probability along ridges (TSI range: 100-180). Again, the high standard deviations do not indicate that changes within each TSI range were extremely variable.
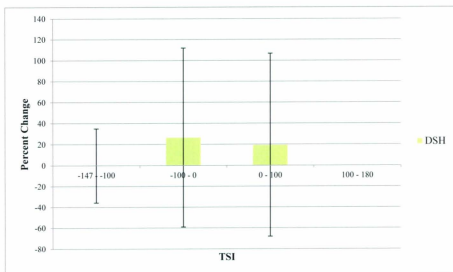
Figure 4.28 Relationship between TSI and percent change in Bayesian probability for deciduous shrub (1983-2008)
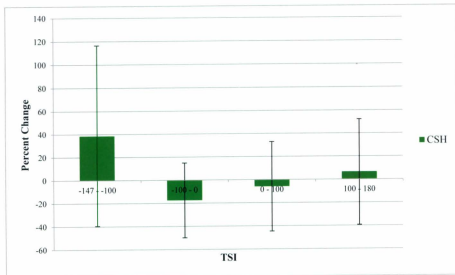
Figure 4.29 Relationship between TSI and percent change in Bayesian probability for coniferous shrub (1983-2008)

4.3 Summary of exploratory analysis findings

This chapter assessed the relationships between each of the land cover classes and the selected topographic variables. Aspect, elevation, and TSI were analysed, because they provide the strongest relationships within each land cover class. The percent change in Bayesian probability between 1983 and 2008 was calculated for the deciduous and coniferous shrub classes. The shrub classes were chosen because they are more heterogeneous over space, as they are restricted primarily to the lower elevations, valley floors, and toe slopes. Also, the shrub classes are expected to migrate to new locations over time and provide the most evidence of vegetation shifts.

In general, deciduous shrub is more likely to occur on southeast-facing slopes, while coniferous shrub prefers north and northwest-facing slopes (Figure 4.1 to 4.4). At elevations between 475 m and 600 m, deciduous and coniferous shrubs occupy the majority of the land cover (Figures 4.5 to 4.8). At elevations above 600 m, there was a steady decrease in the area of the two shrub classes, and increases in both the heath and bedrock/exposed land cover classes.

TSI plots (Figure 4.9 to 4.12) indicate that deciduous and coniferous shrubs tend to be situated along valley floors and toe slopes. Further upslope and on ridges, where conditions become more exposed, the shrub classes are considerably less abundant and there is a dominance of heath and bedrock/exposed land cover.

Figures 4.14 to 4.17 display the change in land cover as related to aspect from 1983 to 2008 for each land cover. Beyond 1983, the bedrock/exposed land cover became more abundant on the southeast- and southwest-facing slopes, indicating a decrease in heath (Figure 4.17). All other land covers remained relatively stationary. The heath land cover class increased at almost all elevation ranges (Figure 4.20) from 1983 to 2005, with a small decrease in 2008. Deciduous and coniferous shrub changes less in relation to elevation from year to year.

The percent change in Bayesian probability from 1983 to 2008 (Figures 4.22 and 4.23) suggests that deciduous shrub decreased in the lower elevations. However, small increases on south-facing slopes and along valley floors were evident. Coniferous shrub

increased in the lower elevations and on north-facing slopes, with minimal increases along valley floors.

Figures 4.24 to 4.29 illustrate how Bayesian probabilities change with relation to aspect, elevation, and TSI. The strongest relationships exist with elevation, where it is evident that the Bayesian probability for deciduous shrub increased at lower elevations, while coniferous shrub decreased.

There was a high positive correlation between the average Bayesian probability for heath and the average maximum summer temperatures for each of the climate stations. Bayesian probabilities for coniferous shrub and deciduous shrub both exhibited negative correlations with the climate stations. Bedrock/exposed did not correlate strongly with the climate stations.

The analysis in this chapter was used to validate the CA-Markov model. While only aspect, elevation, and TSI were thoroughly analyzed, the remaining topographic variables (exposure, slope, TRMI and adiabatic rates) were still included in the model. This is because these variables still provide insight regarding vegetation trends, however, they explain less variation in the model.

5. CA-MARKOV MODEL: VALIDATION AND RESULTS

An overview of the cellular automata-Markov chain model is presented in this chapter. The model inputs and data requirements are outlined and the model validation results are presented. The forecasted 2020 and 2032 images are presented with an emphasis on documenting:

1. the potential net change in land covers;
2. the transition to and from specific land covers;
3. the changes detected along valley floors (areas identified as having a high potential for advancement of the shrub classes).

5.1 CA-Markov model inputs and calibration

The pre-processing steps performed in this section follow the data requirements outlined by Eastman (2009). The first step performed in preparing the land cover classifications for the model was filtering, which consists of a mode filter of a user-defined size that is moved across the study area in an effort to generalize the image without a considerable loss of information (Eastman, 2009). In this case, a 3 x 3 (pixel) window was chosen. While the window can be of any size, tests were performed with increasingly large window sizes. However, windows larger than 3 x 3 resulted in a significant loss of information.

Secondly, areas of no data were masked out. This includes all areas of water, cloud, and cloud shadows. Because the Markov chain module requires two images (earlier and later) with identical dimensions, the no-data regions must be the same for

both images. So while the 1983 image's no-data regions are composed of only waterbodies, the 2008 image contains clouds and shadows, which must be masked out of the 1983 image as well.

Eastman (2009) outlined the requirements for the use of suitability layers in the CA-Markov model. One suitability layer is required for each of the four classified images in this study. The Bayesian probabilities were used as suitability layers for this analysis because they indicate the propensity of specified terrain characteristics to be occupied by a particular land cover class.

5.2 Model validation

The purpose of the CA-Markov model validation procedure is to determine how well the model predicts future land cover scenarios. The model validation steps used in this study were as follows:

1. Time periods were chosen for which data was available. In this case, the 1983 and 2001 images were used to project to 2008.

2. A Markov transition area file was created in the Markov chain model using the 1983 and 2001 images.

3. The Markov transition area file was entered into the CA-Markov model.

4. The earlier land cover image corresponded to that used in the Markov chain model (1983).

5. The transition suitability layers were chosen as the set of four Bayesian probability layers for the later of the two images.

6. Land cover conditions were forecasted ahead to 2008. The Bayesian probabilities for 2001 were chosen over 2008 because for the purposes of forecasting Bayesian probabilities will not be known. For model validation, it is assumed that the 2008 conditions are known.

7. The output of the CA-Markov model was a land cover classification for 2008.

A cross tabulation between the predicted land cover for 2008, and the observed conditions for 2008 resulted in a high level of agreement for the coniferous shrub (κ = 0.68) and bedrock/exposed (κ = 0.73) land covers. The deciduous shrub and heath land cover classes perform poorly in comparison to the other two classes (κ = 0.38 and κ = 0.26, respectively). Table 5.1 presents the Kappa index of agreement between the two images. Table 5.2 illustrates how the image pixels were distributed amongst the classes, as well as producer (omission) and consumer (commission) accuracies. Producer's accuracy indicates the probability that a pixel will be correctly classified. Consumer's accuracy represents the probability that a pixel classified on the map actually represents that category on the ground (Jensen, 2005). While the Kappa values for deciduous shrub and heath are both low, the values for coniferous shrub and bedrock/exposed are considerably better than chance.

Table 5.1 Kappa index of agreement measure for the observed and predicted 2008 land cover classification

Land cover Class	Kappa Index of Agreement (κ)
DSH	0.3786
CSH	0.6792
HTH	0.2566
BRK	0.7265
Overall	0.4613

Table 5.2 Cross tabulations for predicted and observed 2008 land cover classification

		Observed				User's Accuracy
		DSH	CSH	HTH	BRK	
Predicted	DSH	30906	7402	6294	793	68.1%
	CSH	17552	32171	7894	1423	54.5%
	HTH	7508	709	22926	5151	63.2%
	BRK	3228	1197	21081	30267	54.3%
	Producer's Accuracy	52.2%	77.6%	39.4%	80.4%	

The classification accuracies for deciduous shrub and heath are low (Table 5.2). A total of 7.0 km^2 (17,552 pixels) were classified as coniferous shrub, when they were supposed to be classified as deciduous. The same is true for heath, where 8.4 km^2 (21,081 pixels) were incorrectly classified as bedrock/exposed. The heath and bedrock/exposed land covers suffer from considerable pixel-mixing, meaning both land covers tend to occupy an area of land less than the resolution of the original satellite imagery. This explains why the producer's accuracy for heath (39.4%) and the user's accuracy for bedrock/exposed (54.3%) are low. The low producer's accuracy of deciduous shrub (52.2%), combined with the low user's accuracy of coniferous shrub (54.5%), indicates that there is pixel-mixing occurring between those classes as well. This is understandable, as these classes occupy similar topographic conditions. Nonetheless, the model did perform well in predicting the coniferous shrub and bedrock/exposed land covers.

Another model validation was performed to assess the importance of the topographic variables analyzed in Chapter 4 only (aspect, elevation, topographic shape index). The CA-Markov model was run in the same fashion as above, however, the Bayesian probabilities used as the transition suitability layers were constructed using a combination of aspect, elevation, and TSI only. This set of Bayesian probabilities is herein referred to as the "reduced" Bayesian probabilities. The output was a 2008 land cover classification.

Table 5.3 lists the KIA for each of the land covers using these "reduced" Bayesian probabilities. Also listed in Table 5.3 are the KIA values for the original Adding the remaining topographic variables resulted in a 20% increase in model accuracy. All classes were affected by the reduced Bayesian probabilities, particularly the bedrock/exposed land cover.

Table 5.3 Kappa index of agreement measure for the observed and predicted 2008 land cover classification ("reduced" Bayesian probabilities)

Land cover Class	Kappa Index of Agreement (κ) for "reduced" Bayesian probabilities	Kappa Index of Agreement (κ) for original Bayesian probabilities	Change in Kappa Index of Agreement (κ)
DSH	0.1132	0.3786	*-0.2654*
CSH	0.3466	0.6792	*-0.3326*
HTH	0.0742	0.2566	*-0.1824*
BRK	0.2158	0.7265	*-0.5107*
Overall	0.2116	0.4613	*-0.2497*

5.3 CA-Markov forecasting

Balzter (2000) and Logofet and Lesnaya (2000) suggest that time homogeneity is a necessary prerequisite for modelling with Markov chains. Therefore, the CA-Markov

model was forecasted to two future time periods: 2020 and 2032. This represents a maximum of 24 years beyond the 2008 image.

The Markov chain model was run with the images from 1983 and 2008. A 12-year projection was performed to obtain transition probabilities for 2020. The *Markov transition areas* file was used in the CA-Markov model. The earlier land cover image was set as the 1983 image. The Bayesian probabilities for 2008 were set as the suitability image collection. Although it may have seemed more logical to use the 1983 Bayesian probabilities as the suitability image collection, the 2008 probabilities represented the most recent land cover conditions and were more accurately classified than the 1983 imagery. Also note that the Markov chain analysis was performed between 1983 and 2008. Therefore, the transition matrix would represent trends present between these two time periods. The number of CA iterations was equal to the number of years the Markov chain was projected forward, in this case 12 years. Also, recall that the most noticeable changes are evident over decadal time scales (Pereg and Payette, 1998; Epstein *et al.*, 2004; Stow *et al.*, 2004; IPCC, 2007).

This procedure was performed again with a change in the time scale to allow a projection to 2032. The projection in the Markov model was for 24 years, and 24 CA iterations in the CA-Markov model.

The Markov chain model produced two sets of outputs; one each for the 2020 projection and the 2032 projection. Of interest from these outputs are the Markov transition probability files. These highlight the propensity for a particular land cover to

stay the same, or transition to another land cover class. Table 5.4 and 5.5 list the
transition probabilities for the 2020 and 2032 projections, respectively.

Table 5.4 Markov transition probabilities for projection to 2020

		Probability of Changing to:			
		DSH	CSH	HTH	BRK
Given:	DSH	**0.7717**	0.0932	0.1351	0.0000
	CSH	0.2523	**0.6503**	0.0973	0.0000
	HTH	0.0988	0.0000	**0.5780**	0.3232
	BRK	0.0307	0.0279	0.4176	**0.5238**

Table 5.5 Markov transition probabilities for projection to 2032

		Probability of Changing to:			
		DSH	CSH	HTH	BRK
Given:	DSH	**0.6691**	0.1228	0.1868	0.0214
	CSH	0.3195	**0.5078**	0.1460	0.0268
	HTH	0.1352	0.0143	**0.5214**	0.3291
	BRK	0.0807	0.0357	0.4314	**0.4523**

Table 5.4 illustrates that in 2020 there was a 77% chance of deciduous shrub
remaining as such, with less than a 10% chance of it transitioning to coniferous shrub,
and a 13% chance of it transitioning to heath. The tendency is for coniferous shrub to
remain the same as well (65%). There is a 25% chance of it changing to deciduous shrub.
This type of transition is expected given the close proximity of deciduous and coniferous
shrub. Due to the patchy nature of heath, the probabilities of change for the heath and
bedrock/exposed land covers are less pronounced. There is only a 58% chance of heath
remaining heath, with a 32% chance of it changing to bedrock. Bedrock has a 52%
chance of remaining the same, with a 41% chance of it being overtaken by heath.

Increasingly long Markov chain projections result in transition probabilities approaching equilibrium. While the probabilities listed in Table 5.5 have not reached equilibrium, they are trending toward it. The probabilities of classes remaining the same were lower. There was a 67% chance of deciduous shrub remaining the same, and a 51% chance of coniferous shrub remaining the same. There remains significant mixing between the heath and bedrock/exposed land cover classes. When the transition probabilities reach equilibrium, it does not mean the landscape will stop changing; rather, it is an indication that the Markov chain is no longer able to make accurate predictions given the amount of data available.

5.4 CA-Markov model results

Figure 5.1 and 5.2 illustrate the forecasted land cover conditions to 2020 and 2032, respectively.

5.4.1 Net change in land cover

It is important to assess the outputs of the model and determine what has changed from the baseline conditions (2008) to the predicted conditions (2020 and 2032). Over the first time step (2008 to 2020), coniferous shrub and bedrock both increased (by 7.3 and 5.7 km^2, respectively). Deciduous shrub and heath both decreased over this time period (by 6.5 and 6.4 km^2, respectively). Figure 5.3 shows the net change for each land cover class between 2008 and 2020. Figure 5.4 presents the net change from 2008 to 2032. Coniferous shrub and bedrock/exposed are no longer expanding, in fact, they experienced a decrease beyond 2020 (bedrock/exposed was likely replaced by heath in

this time period). Deciduous shrub and heath, while still considerably less abundant than in 2008, increased beyond 2020.

The increases in coniferous shrub, combined with the high transition probability of coniferous shrub to remain the same in 2020 (0.6503) (Table 5.4) provides strong evidence that coniferous shrub is the more resilient of the land cover classes. Deciduous shrub had a high transition probability (0.7717) to 2020, as well. However, the large decrease illustrated in Figures 5.1 and 5.2 suggest it is less resilient than coniferous shrub.

Land Cover Class

Deciduous Shrub	No Data	
Coniferous Shrub	Waterbodies	
Heath	Approximate Treeline (1950 aerial imagery)	
Bedrock/Exposed		

N

0   1,000   2,000 Meters
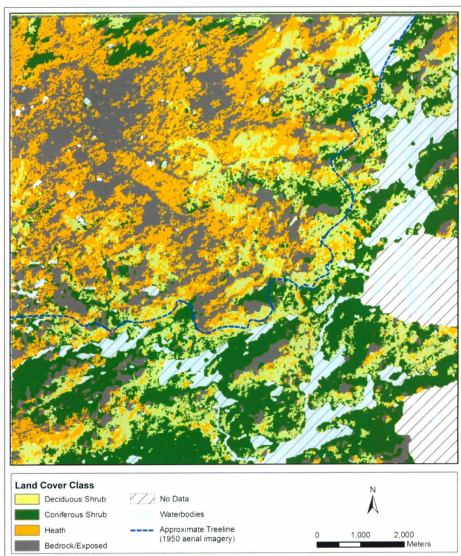
Figure 5.1 CA-Markov land cover projection (2020)

Land Cover Class

- Deciduous Shrub
- Coniferous Shrub
- Heath
- Bedrock/Exposed
- No Data
- Waterbodies
- Approximate Treeline (1950 aerial imagery)

N

0   1,000   2,000
Meters
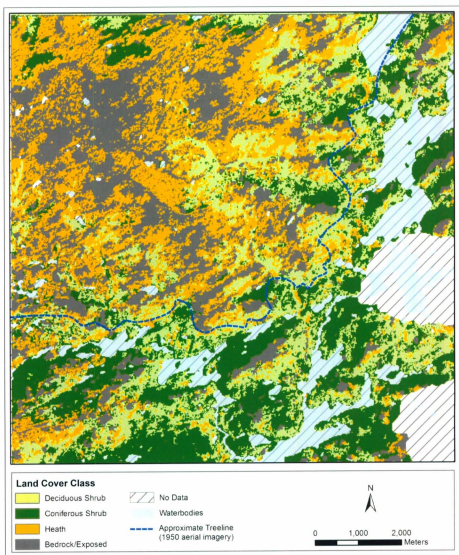
Figure 5.2 CA-Markov land cover projection (2032)
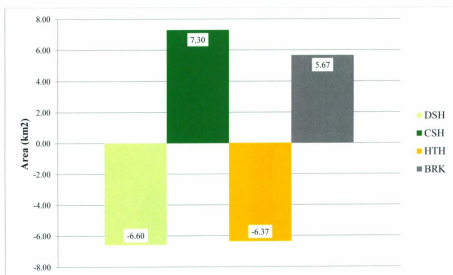
Figure 5.3 Gains and losses by land cover class (2008-2020)
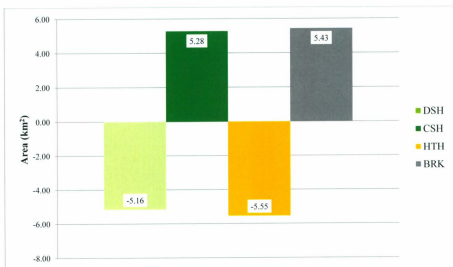
Figure 5.4 Gains and losses by land cover class (2008-2032)

5.4.2 Net change within land cover classes

The contributions from each class to the gains or losses in a target class provide a good indication as to what classes tend to exchange area. In this study, deciduous and coniferous shrubs tend to exchange pixels in the forecasted images. This is to be expected, given the ecological similarities and close spatial proximity of the two classes. Heath and bedrock/exposed also exchanged area between the baseline image and the forecasted images. The exchanges between heath and bedrock/exposed relate to the patchy nature of these land covers.

Figure 5.5 outlines the contributors to net change for each of the land cover classes from 2008 to 2020. Each graph contains three values, one for each of the land covers that are contributing to the change in the fourth land cover, which is excluded from the graph. When examining these graphs, it is important to note how the land cover changed in the time period of interest. Deciduous shrub decreased from 2008 to 2020 by 6.6 km^2; 4.82 km^2 of this area was replaced by coniferous shrub (Figure 5.5, Graph 1). Heath also decreased by 6.37 km^2 in this time period with 4.04 km^2 being lost to bedrock/exposed (Figure 5.5, Graph 3).

Figure 5.6 presents the contributors to net change from 2020 to 2032. Again, deciduous and coniferous shrubs tend to exchange area (Figure 5.6, Graphs 1 and 2), as does heath and bedrock/exposed (Figure 5.6, Graphs 3 and 4). The severity of the changes seen in these graphs is mimicked in the transition probabilities to 2032, which are less pronounced than the transition probabilities to 2020.
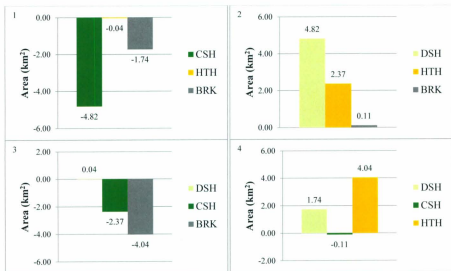
Figure 5.5 Net change within land cover classes (2008-2020) (1-DSH, 2-CSH, 3-HTH, 4-BRK)
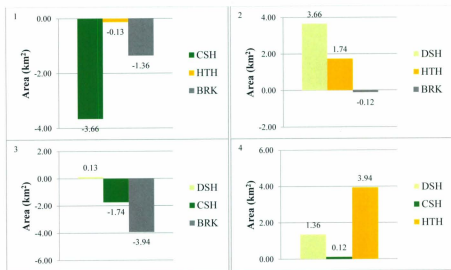
Figure 5.6 Net change within land cover classes (2008-2032) (1-DSH, 2-CSH, 3-HTH, 4-BRK)

The trends present in Figures 5.5 and 5.6 support the transition probabilities presented in Table 5.4 and 5.5. The Markov transition probabilities suggest that if deciduous shrub were to transition to another land cover, it would most likely be coniferous shrub, and vice versa. The same is true for the heath and bedrock/exposed land covers. Given the Markov transition probabilities, which indicate how land covers are expected to change over time, the trends present in Figures 5.5 and 5.6 are expected.

5.4.3 Land cover change along valley floors

The relative degree of predicted change seen along the valley floors from 2008 to 2020, and from 2020 to 2032, is less than was evident from 1983 to 2008. Observing the changes from 2008 to 2020, it is evident there was a small amount of infilling and upslope movement along valley floors. The majority of the growth in coniferous shrub occurred in the lower elevations of the study area. As mentioned, deciduous shrub decreased in this time period, however, a majority of the area was replaced by coniferous shrub. At lower elevations and along valley floors, deciduous and coniferous shrub experienced small amounts of infilling and upslope movement ($\sim$4.5 km^2), primarily at fringe or boundary areas. These changes are consistent with those detected from 1983 to 2008. While there was considerable fluctuation in land covers in the historic images, a general progression of deciduous and coniferous shrub along valley floors was witnessed.

From 2020 to 2032, infilling at low elevations and along valley floors is less distinct ($\sim$2.0 km^2). There is, however, some infilling of deciduous shrub along the valley floors. There were minimal changes in coniferous shrub. At lower elevations, coniferous shrub was replaced by deciduous shrubs at fringe areas between the two classes. Heath

increased from 2020 to 2032. These changes were seen on the fringe areas of deciduous shrub, where the valley floors begin transitioning into toe slopes and elevations become too extreme for shrub growth.

5.5 Overview of results

The validation model performed well in predicting the occurrence of coniferous shrub and bedrock/exposed (Table 5.1). The validation process was a necessary step to justify the use of the CA-Markov model. The forecasted images show an increase in coniferous shrub and bedrock/exposed (indicating a decrease in heath) from 2008 to 2020. While deciduous shrub decreased in this time period, it did experience minimal upslope movement along valley floors and toe slopes. Coniferous shrubs increased considerably in the lower elevations, with minimal gains along valley floors. Deciduous shrubs increased along valley floors to 2032. Heath also increased to 2032, primarily at the fringe areas of deciduous shrub in the valley floors and toe slopes. Coniferous shrub lost a small amount of its area in the lower elevation to deciduous shrub from 2020 to 2032.

6. DISCUSSION

This chapter presents a summary of the climate interpolation as well as the changes observed from 1983 to 2008. An overview of the trends detected by the exploratory data analysis is given, with an explanation of the implications these results have on model development. A review of the methods, model results, and model implications will follow. Finally, an outline of the project findings in relation to the project objectives is given.

6.1 Climate change

Regional climate data for Goose Bay (1942-2008) and Cartwright (1941-2007) were used in conjunction with localized data from the Mealy Mountains dating from 2001 to 2007. This combination of data was used to interpolate a long running set of local climate data spanning the dates of the imagery (1983-2008).

From 1983 to 2008, temperatures at the upper and lower climate stations increased in the same manner as the regional data derived from Goose Bay and Cartwright. There was an increase of approximately 1.2° C from 1983-2001, with a period of increased warming from 2001-2008, where temperatures increased 1.0° C. Recognizing these important temperature fluctuations is necessary to understand the cause of past and future land cover changes. These temperature shifts have important consequences on vegetation growth, particularly regarding the upslope movement of deciduous and coniferous shrub. While it is difficult to determine exactly what caused the observed and predicted changes in land cover, a literature review has indicated that climate and topography are strongly

associated with vegetation migration (Körner and Paulsen, 2004; Lloyd and Fastie, 2002; MacDonald *et al.*, 2008; Payette and Delwaide, 1994).

6.2 Exploratory data analysis

Exploratory analysis was performed to determine the relationships between the land cover classes and topographic variables, climate patterns, and Bayesian probabilities. The purpose of this analysis was to test the suitability of these variables for predicting future scenarios within the CA-Markov model.

The exploratory data analysis revealed a preference for deciduous shrubs to occupy southeast-facing slopes, while coniferous shrubs preferred north- and northwest-facing slopes. The two shrub classes dominate the lower elevations, while heath and bedrock/exposed occupy the majority of the upper elevations.

It is, however, the mid-elevations where considerable mixing of all four classes occurred. Valley floors in particular have been the site of advancement of the shrub classes from 1983 to 2008. At higher elevations, heath and bedrock/exposed continued to be the dominant land covers.

Between 1983 and 2008, there was no considerable change in the land covers with relation to topographic conditions (*e.g.* deciduous shrub did not move to more exposed slopes, coniferous shrub did not move to higher elevations, *etc.*). However, observation of the land cover images reveals a movement of coniferous and deciduous shrub along the valley floors, suggesting there was some movement of land cover classes. These changes

were not detected in the exploratory analysis because the changes were relatively small in comparison to the entire range of aspect, elevation, and TSI values.

Another important conclusion obtained from the exploratory analysis relates to the Bayesian probabilities. The probability of the shrub classes, particularly deciduous shrub, increased along the valley floors, suggesting that infilling has occurred. Coniferous shrub increased primarily in the lower elevations (<550 m).

6.3 Review of methods and results

A cellular automata-Markov chain (CA-Markov) hybrid model was used to forecast land cover conditions to 2020 and 2032. The forecast model does not go beyond 2032 (a 24-year time range) due to the restriction of time homogeneity in these particular models.

Model validation was performed to determine how well the CA-Markov model predicts future conditions. The validation results indicated that the coniferous shrub class predicted moderately well. Heath is predicted relatively poorly; however bedrock is predicted much more accurately. This discrepancy is due to the patchy nature of heath and bedrock/exposed, whereby both land covers occupy the same pixel, producing a mixed spectral signature.

From 2008 to 2032, the transition probabilities decrease. The gains in coniferous shrub and bedrock/exposed began to decrease, while the losses in deciduous shrub and heath decreased as well. The most noticeable changes occurred in the fringe areas between deciduous shrub and heath. Coniferous shrub continued to increase at lower

elevations, but decreased along the valley floors. Heath re-emerged where topographic conditions became more exposed (at the mid-slopes and ridge tops).

The changes to and from the land cover classes discussed in Chapter 5 provide important information regarding the dynamics of land covers in the area. The general trend suggests that deciduous and coniferous shrub tend to experience gains and losses to and from one another. The same is true for heath and bedrock. This is expected for two reasons. The first relates to pixel-mixing, especially between the heath and bedrock/exposed land covers, but also partially to the deciduous and coniferous shrub classes. Pixel-mixing is most common where land covers exhibit a patchy nature. This is most evident with the heath land cover. The second reason relates to the spatial arrangement of the classes. For the most part, deciduous shrub and coniferous shrub, and heath and bedrock/exposed, occur in close proximity to one another. As a result, these classes are expected to exchange area with one another. In the early stages of model development, a model was constructed with deciduous and coniferous shrub combined into a single class. The results, however, were similar to the current model. Merging the classes provided a less detailed projection, while providing no further accuracy.

The concept of vegetation succession should also be mentioned here. Meades (1983) points out that the progression from heath to forested land covers in climates such as those typical to Newfoundland and Labrador tends to be very slow. The author concludes that it would take forested areas approximately 1000 years to completely overtake an area of heath approximately 2-3 ha in size. However, the author does state that small shrub growth is present within the heath land cover. The conclusions reached

by Meades (1983) suggests that the progression of land covers within this study are logical, in that heath will subside to the forested land covers of deciduous and coniferous shrub.

6.4 Model implications

A visual assessment of past and future classified images indicates that deciduous shrubs are advancing and infilling along valley floors and toe slopes, but decreasing in the lower elevations. These changes are particularly evident at mid-elevations. The valley floors and toe slopes offer more protected conditions, and are thus favourable to the advancement of certain land cover types. Coniferous shrub also emerges along the valley floors, however it is less prominent. The lower elevations are more likely to experience an increase in coniferous shrub where old growth forests constitute the majority of the landscape. These conditions are expected to become more pronounced into the future as well. The infilling of deciduous and coniferous shrub suggests that these land covers will become more abundant and eventually begin to move upslope as conditions at higher elevations and exposed slopes become more hospitable to growth (Gamache and Payette, 2005).

The study area falls within the boundaries of the Mealy Mountains (*Akamiuapishku*) National Park. The conclusions reached in the above analysis have important consequences for land planning and park management, especially with regards to indigenous populations that use the area. This study provides a generalisation of past and potential future changes in vegetation patterns; changes which should be considered, and more thoroughly investigated, if further land management and zoning is to occur in

the area. Additionally, the predicted changes could have important impacts on wildlife in the area. Changes in land cover patterns could potentially alter migration patterns of caribou which frequent the area.

6.5 Review of project objectives

This section reviews the project objectives and addresses each individually in the relation to the conclusions reached in this study.

6.5.1 Mapping historical land cover distributions

The past land cover classifications provide important information regarding the trends which have occurred over the past 25 years (1983-2008). This information is crucial in developing future vegetation scenarios.

While the classification accuracies appear relatively low, especially for the older images, there are explanations for this. First and foremost, the quantifiable field data used to create training and testing sites was used in conjunction with qualitative user knowledge, for which there is no numerical equivalent. So while the accuracies are low, the combination of field data and user knowledge was adequate in classifying the images. In addition, training sites were developed for 2008 and used on all images. Thus, in 1983, for example, land cover conditions are expected to be somewhat different because the ground truth points are those developed for 2008.

6.5.2 Relating land cover change to climatic fluctuations

While it is difficult to see a direct correlation between the quantity of a particular land cover and the climatic conditions at the time, a thorough literature review suggests that

increases in temperature do in fact have an effect on vegetation patterns. The movement of deciduous and coniferous shrub along valley floors and into toe slopes occurs in conjunction with an increase in temperature of approximately 2 °C over the 25-year time frame of this study. Changes in Bayesian probabilities from 1983 to 2008 are minimal, suggesting infilling is occurring at a slow rate, and most changes are occurring along fringe areas where shrubs are beginning to move upslope. These climate changes are expected to continue into the future, thus it is reasonable to assume that land cover shifts will occur as well. Additionally, average Bayesian probabilities exhibited strong correlations with average maximum summer temperatures, particularly coniferous shrub and heath.

While the Bayesian probabilities (used in the CA-Markov model) include an adiabatic rate layer, the final model does not directly incorporate a climate change vector. Nonetheless, the model does effectively incorporate the changes that occurred in land cover between 1983 and 2008, which, as discussed, are strongly associated with changes in climate.

6.5.3 Identifying topographic conditions specific to land cover classes

The exploratory analysis section was important in justifying the use of a spatial model. Early modelling attempts explored the notion of logistic regression, however, it was determined that a spatial component had to be included to capture the true variability of the landscape. Given the use of the CA-Markov model, which incorporates a spatial component, it was necessary to know the dynamics of the land cover classes in relation to the topographic variables.

A CA-Markov model was run using "reduced" Bayesian probabilities compiled from only aspect, elevation, and topographic shape index. Because these three variables showed the greatest variability amongst the land cover classes, they provided the greatest predictive power to the model, and were thus chosen for exploratory analysis. Given the movement of deciduous and coniferous shrub along valley floors and toe slopes, aspect, elevation, and TSI were also the most logical choice for further analysis because they offered unique values for these areas. The CA-Markov model performed with the "reduced" Bayesian probabilities proved that using only aspect, elevation, and TSI as predictive variables decreased the model's accuracy considerably. Including all topographic variables increased model accuracy by approximately 20%.

6.5.4 Forecasting future land cover conditions

A CA-Markov model was used to forecast potential future land cover conditions. The appeal of this model comes from its ability to incorporate the past states of systems (via the Markov chain), as well as the spatial organization of the system (via the cellular automata). These characteristics give the CA-Markov model a spatial and temporal framework.

Various other model types were tested, with results proving less favourable. A Geographically Weighted Logistic Regression (GWLR) was tested in the earlier stages of analysis; however, this model was unable to capture the trends occurring in the data, likely because of an overgeneralization of neighbourhoods and the failure of the data to meet the condition of spatial non-stationarity. A spatial auto-regressive model was tested

106

briefly, as well. While the inclusion of a spatial term was beneficial, the regression functions did not properly capture the trends in the data.

The changes detected from 1983 to 2008 suggest an upslope movement of shrubs, particularly deciduous, along valley floors and into toe slopes. These shifts continue into the forecasted land cover conditions, though to a lesser degree. In the observed and forecasted land cover maps, deciduous shrub appears to be at the fringe areas of upslope movement (particularly along the valley floors). This may suggest a tendency for deciduous shrub to move upslope ahead of coniferous shrub.

6.6 Conclusion

This study provides an assessment of the continuously changing vegetation patterns of forest-tundra ecotones. The multi-temporal satellite imagery provides the basis of the study. Bayesian probabilities, which have not been used extensively in ecological studies, provide suitability measurements for each of the land cover classes in relation to topographic variables.

To fully understand the changes which have taken place in the Mealy Mountains, particularly along the forest-tundra ecotone, additional work should be undertaken. Future studies should focus on obtaining a more complete record of imagery for the area. The imagery used in this study covered a long time frame (25 years), but there were considerable gaps, especially between the 1983 and 2001 image (early in this study, a 1992 image was used, but it was later dropped due to only 50% of the image being cloud free). While consistent, high-resolution imagery isn't always available, it should be chosen when feasible. This will prevent the loss of information when down-scaling high

resolution images to match lower resolution imagery. Alternatively, high-resolution, multi-spectral airborne imagery could be obtained at various time frames. RADAR imagery could be used as supplemental data to the analysis in the form of texture analysis. Finally, a more complete, localised record of climate would be ideal. However, considering the study should be carried out over multiple decades in order to capture significant shifts in vegetation, these data may not always be available.

7. REFERENCES

Balzter, H. (2000) Markov chain models for vegetation dynamics. *Ecological Modelling* *126*, 139-154.

Balzter, H, Braun, P.W., & Köhler, W. (1998) Cellular automata models for vegetation dynamics. *Ecological Modelling 107*, 113-125

Benabdellah, B., Albrecht, K.-F., Pomaz, V.L., Denisenko, E.A., & Logofet, D.O. (2003) Markov chain models for forest successions in Erzebirge, Germany. *Ecological Modelling 159*, 145-160.

Bonham-Carter, G.F. (1994) *Geographic information systems for geoscientists: modelling with GIS.* The Netherlands: Pergamon.

Borsuk, M.E., Reichert, P., Peter, A., Schager, E. & Burkhardt-Hilm, P. (2006) Assessing the decline of brown trout (*Salmo trutta*) in Swiss rivers using a Bayesian probability network. *Ecological modelling 192*, 224-244.

Byrne, G.F., Crapper, P.F., Mayo, K.K. (1980) Monitoring land-cover change by principal component analysis of multitemporal Landsat data. *Remote Sensing of Environment 10*, 175-184

Caley, P., Groves, R.H., Barker, R. (2008) Estimating the invasion success of introduced plants. *Diversity and Distributions 14*, 196-203.

Canadian Institute of Climate Studies (CICS) (2003) Retrieved December 18, 2008. http://www.cics.uvic.ca/.

Carmel, Y., & Kadmon, R. (1999) Effects of grazing and topography on long-term vegetation changes in a Mediterranean ecosystem in Israel. *Plant Ecology 145*, 243-254.

Chen, W., Armenakis, C., Blain, D., Brook, R., Cyr, I., McDonald, K., Dyke, L., Fernandes, R., Fraser, R., Grieve, S., Hamilton, K., Héile, R., Johnson, V., Koehler, K., Latifovic, R., Leblanc, S., Li, J., McLemman, D., Moghaddam, M., Olthof, I., Perrott, T., Sladen, W., Valleau, R., Wang, J., Wang, S., Wu, W., Zhang, Y., & Zhang, Y. (2007) *IPY CiCAT Field Measurement Protocol for Mapping Canada's Arctic Vegetation, version 4.0.* Unpublished.

Collins, L. (1975) *An introduction to Markov chains analysis.* London, United Kingdom: Headley Brothers Ltd.

Cornwall, C., Horiuchi, A., & Lehman, C. (2008) *Solar position calculator*. National Oceanic and Atmospheric Administration (NOAA), Earth Systems Research Laboratory. http://www.srrb.noaa.gov/highlights/sunrise/azel.html

Czárán, T., & Sándor, B. (1992) Spatiotemporal dynamic models of plant populations and communities. *TREE 7*(2), 38-42.

De Smith, M.J., Goodchild, M.F., & Longley, P. (2007) *Geospatial analysis: a comprehensive guide to principles, techniques and software tools, 2nd edition.* Leicester, UK: The Winchelsea Press.

Eastman, J.R. (2009) *IDRISI Taiga: guide to GIS and image processing, version 16.02.* Worcester, MA: Clark University.

Eastman, J.R. (2009) Idrisi Taiga [computer software]. Worcester, MA: Clark University.

Epstein, H.E., Calef, M.P., Walker, M.D., Chapin III, F.S., & Starfield, A.M. (2004) Detecting changes in arctic tundra plant communities in response to warming over decadal time scales. *Global Change Biology 10*, 1325-1334.

Environment Canada (2009) National Climate Data and Information Archive. Retrieved February 3, 2009. http://climate.weatheroffice.gc.ca/climateData/canada_e.html

European Commission (2010). SOTER Model. Joint Research Council, Institute for Environment and Sustainability. Retrieved January 15, 2010). http://eusoils.jrc.ec.europa.eu/projects/SOTER/SOTER_model.html.

Gamache, I., & Payette, S. (2005) Latitudinal response of subarctic tree lines to recent climate change in eastern Canada. *Journal of Biogeography 32*, 849-862.

Hanson, B. (1987) Reconstructing mass-balance profiles from climate for an Arctic ice cap. *The Physical Basis of Ice Sheet Modelling* (Proceedings of the Vancouver Symposium), IAHS Publ. no. 170.

Harrison, S.J., & Kelly, I. (1996) A field-based index of topographic shelter and its application to topoclimatic variation. *Applied Geography 16*(1), 53-63.

Hayes, D.J., Sader, S.A. (2001) Comparison of change-detection techniques for monitoring tropical forest clearing and vegetation regrowth in a time series. *Photogrammetric Engineering and Remote Sensing 67*(9), 1067-1075.

Holland, P.G., & Steyn, D.G. (1975) Vegetational responses to latitudinal variations in slope angle and aspect. *Journal of Biogeography 2*(3), 179-183.

110

Huntley, B. (1991) How plants respond to climate change: migration rates, individualism and the consequences for plant communities. *Annals of Botany 67* (supplement 1), 15-22.

IPY (2005) International Polar Year Objectives. Retrieved February 5, 2011. http://classic. ipy.org/development/objectives.htm.

IPCC (2007) Climate Change 2007: Synthesis Report. Contribution of Working Groups I, II, and III to the Fourth Assessment Report of the Intergovernmental Panel on Climate Change. In P.R. [Core Writing Team (ed.). (p. 104)]. Geneva, Switzerland: IPCC.

Jacobs, J. (2007) Climate studies in the Mealy Mountains. *Labrador Highlands Research Group, Report of Research 2006* (Memorial University, Department of Geography, St. John's, NL.)

Jano, A.P., Jefferies, R.L., & Rockwell, R.F. (1998) The detection of vegetational change by multitemporal analysis of LANDSAT data: the effects of goose foraging. *Journal of Ecology 86*, 93-99.

Jensen, J.R. (2005) *Introductory digital image processing: a remote sensing perspective, 3rd ed.* Toronto, Canada: Pearson Prentice Hall.

Keith, T. (2001). *A Natural History and Resource Inventory of the Proposed Mealy Mountains (Akamiuapishku) National Park Study Area, Labrador*. Park Establishment Branch, Parks Canada.

Körner, C. & Paulsen, J. (2004) A world-wide study of high altitude tree line temperatures. *Journal of Biogeography 31*, 713-732.

Lippe, E., De Smidt, J.T., & Glenn-Lewin, D.C. (1985) Markov models and succession: a test from a heathland in the Netherlands. *Journal of Ecology 73*(3), 775-791.

Lloyd, A.H., & Fastie, C.L. (2002) Spatial and temporal variability in the growth and climate response of tree lines in Alaska. *Climatic Change 52*, 481-509.

Logofet, D.O., & Lesnaya, E.V. (2000) The mathematics of Markov models: what Markov chains can really predict in forest succession. *Ecological Modelling 126*, 285-298.

MacDonald, G.M., Kremenetski, K.V., & Beilman, D.W. (2008) Climate change and the northern Russian tree line zone. *Philosophical Transactions of the Royal Society B: Biological Sciences 363*, 2285-2299.

Marshall, E., & Randhir, T.O. (2008) Spatial modeling of land cover change and watershed response using Markovian cellular automata and simulation. *Water Resources Research 44*, 1-11.

Malcolm, J.R., Makrham, A., Neilson, R.O., & Garaci, M. (2002) Estimated migration rates under scenarios of global climate change. *Journal of Biogeography 29*, 835-849.

McClave, J.T., & Sincich, T. (2000) *Statistics 8th ed.* Upper Saddle River, NJ: Prentice Hall.

McNab, W.H. (1989) Terrain shape index: quantifying effect of minor landforms on tree height. *Forest Science 35*(1), 91-104.

Meades, S. (1990) *Natural regions of Newfoundland and Labrador*. St. John's, NF: Protected Areas Association.

Meades, S. (1982) The origin and successional status of anthropogenic dwarf shrub heath in Newfoundland. *Advances in Space Research 2*(8), 97-101.

Miller, L. (2005) Incorporating spatial dependence in predictive vegetation models: residual interpolation methods. *The Professional Geographer 57*(2), 169-184.

Mitchell, K. (2007) *Quantitative analysis by the Point-Centered Quarter Method*. Department of Mathematics and Computer Science, Hobart and William Smith Colleges. http://people.hws.edu/mitchell/PCQM.pdf

Myneni, R.B., Hall, F.G., Sellers, P.J., Marshak, A.L. (1995) The interpretation of spectral vegetation indexes. *IEEE Transactions on Geoscience and Remote Sensing 33*(2): 481-486.

Natural Resources Canada (2010). National Topographic Data Base (NTDB). http://geogratis.cgdi.gc.ca/geogratis/en/index.html.

Parker, A.J. (1982) The topographic relative moisture index: an approach to soil moisture assessment in mountain terrain. *Physical Geography 3*(2): 160-168.

Payette, S. (2007) Contrasted dynamics of northern Labrador tree lines caused by climate change and migrational lag. *Ecology 88*(3), 770-780.

Payette, S., & Delwaide, A. (1994) Growth of Black Spruce at its northern range limit in Arctic Quebec, Canada. *Arctic and Alpine Research 26*(2), 174-179.

Pereg, D., & Payette, S. (1998) Development of black spruce growth forms at tree line. *Plant Ecology 138*, 137-147.

Phipps, M.J. (1992) From local to global: the lesson of cellular automata. In DeAngelis, D.L., Gross, L.J. (eds.), *Individual-based models and approaches in ecology: populations, communities and ecosystems.* New York, NY: Chapman and Hall.

Rupp, T.S., Chapin III, F.S., & Starfield, A.M. (2001) Modeling the influence of topographic barriers on treeline advance at the forest-tundra ecotone in northwestern Alaska. *Climatic Change 48*, 399-416.

United States Geological Survey (2010). Shuttle Radar Topography Mission. http://srtm.usgs.gov/index.php

United States Geological Survey (2010). Project Documentation. http://landsat.usgs.gov/tools_project_documents.php

Stow, D.A., Hope, A., McGuire, D., Verbyla, D., Gamon, J., Huemmrich, F., Houston, S., Racine, C., Sturm, M., Tape, K., Hinzman, L., Yoshikawa, K., Tweedie, C., Noyle, B., Silapaswan, C., Douglas, D., Griffith, B., Jia, G., Epstein, H., Walker, D., Daeschner, S., Petersen, A., Zhou, L., & Myneni, R. (2004) Remote sensing of vegetation and land-cover in arctic tundra ecosystems. *Remote Sensing of Environment 89*, 281-308.

Treml, V., & Banaš, M. (2008) The effect of exposure on alpine tree line position: a case study from the High Sudetes, Czech Republic. *Arctic, Antarctic, and Alpine Research 40*(4), 751-760.

Usher, M.B. (1981) Modelling ecological succession, with a particular reference to Markovian models. *Vegetatio 46/47*, 11-18.

Wolfram, S. (1983) Statistical mechanics of cellular automata. *Reviews of Modern Physics 55*(3), 601-644.

Zimmerman, N. (2000) *Tools for analyzing, summarizing, and mapping of biophysical variables.* Retrieved September 22, 2009. http://www.wsl.ch/ staff/ niklaus.zimmermann/programs/aml4_2.html.

APPENDIX A

The table below (Table A1) lists the type (Quad: Quadrat; PCQ: Point-Centre Quarter) and X and Y values for each of the field points collected during the summer of 2008.

Table A1 Quadrat and PCQ field points

Survey Type	X (Easting)	Y (Northing)	Survey Type	X (Easting)	Y (Northing)
Quad	375888	5940452	Quad	376780	5941432
Quad	380732	5943776	Quad	377019	5941371
Quad	380135	5940188	Quad	378730	5941586
Quad	377183	5938873	Quad	379019	5943324
Quad	376072	5939985	Quad	376493	5942078
Quad	375877	5939765	Quad	376606	5941595
Quad	379144	5942444	Quad	377825	5938681
Quad	379937	5940354	Quad	376424	5941513
Quad	376464	5939972	Quad	378475	5943254
Quad	381901	5942199	Quad	378378	5942665
Quad	375819	5939626	Quad	379873	5940415
Quad	375835	5940031	Quad	376365	5939632
Quad	378745	5938873	Quad	375726	5941408
Quad	379231	5942093	Quad	380017	5943171
Quad	378359	5938663	Quad	378786	5941402
Quad	380309	5944195	Quad	378712	5943322
Quad	379656	5941824	Quad	375789	5943711
Quad	379678	5942576	Quad	376358	5943381
Quad	379336	5942539	Quad	378184	5940658
Quad	379317	5940421	Quad	377927	5940236
Quad	377558	5940686	Quad	378314	5941220
Quad	375993	5942604	Quad	377828	5941774
Quad	376151	5941183	PCQ	381449	5942550
Quad	376203	5942698	PCQ	380220	5941873
Quad	376271	5941716	PCQ	381817	5940926
Quad	375982	5942959	PCQ	381652	5942459
Quad	378196	5943403	PCQ	380846	5941221
Quad	378164	5942888	PCQ	380865	5942122

Table A1 *cont'd*

Survey Type	X (Easting)	Y (Northing)	Survey Type	X (Easting)	Y (Northing)
Quad	377805	5942335	PCQ	377447	5938735
Quad	376201	5942477	PCQ	380947	5939863
Quad	379129	5940955	PCQ	381828	5941293
Quad	378791	5941316	PCQ	381078	5939765
Quad	380101	5943796	PCQ	381286	5941033
Quad	379656	5943374	PCQ	381132	5939642
Quad	380209	5944056	PCQ	380773	5942102
Quad	379937	5940788	PCQ	380561	5941674

APPENDIX B

The following details the specifics of the geometric, atmospheric, and radiometric correction procedures applies to the four multi-date satellite images used in this analysis.

Re-sampling and georeferencing

For the purposes of this analysis, the 2001 image was re-sampled to a 20 m resolution and used as a basis for all other correction performed. The 2001 image was chosen as the reference image because it was previsouly georeferenced by the image provider. The remaining images (1983, 2005, and 2008) were re-sampled to 20 m resolutions as well.

The 1983, 2005, and 2008 images were georeferenced using the 2001 image and a topographic mapsheet water polygon layer to create ground control points (GCP). The table below shows the root-mean square (RMS), mapping function, and re-sampling type used for each image.

Table B1 RMS, mapping function, and re-sampling type for imagery

	1983	2005	2008
Mapping function	Cubic	Quadratic	Quadratic
RMS	0.455	3.341	0.647
Number of GCPs	16	12	15
Resampling type	Bilinear	Nearest Neighbour	Nearest Neighbour

Atmospheric correction

Atmospheric correction was applied to all bands from each image year using the dark object subtraction method. This method involves reducing the darkest pixel in an image

to a brightness value of 0 (Jensen, 2005). To complete this procedure, the ATMOSC module in *Idrisi Taiga* was used. The date and time of each satellite image was retrieved from the images header file, the band centre wavelengths were found in Jensen (2005). The DH Haze was estimated using the lowest value in the histogram of each band of each image. The L-min and L-max for the 2008 image were found in the images header file. For the 1983 and 2001 image the values were found via the USGS website (2011). Values for the 2005 image were unavailable, so the image was not calibrated. The solar spectral irradiance was calculated within *Idrisi Taiga* using the image capture time and wavelength of the band centre. The sun elevation was calculated using the sun position calculator produced by the National Oceanic and Atmospheric Administration (NOAA) (2008). Table B2 to B4 list the atmospheric correction parameters for the 1983, 2001, and 2008 images, respectively.

Table B2 Atmospheric correction parameters for 1983 image

	Band 1	Band 2	Band 3
Date (mm/dd/yy)	7/24/1983	7/24/1983	7/24/1983
Time (GMT)	14:22:41	14:22:41	14:22:41
λ of band centre (μm)	0.55	0.65	0.75
DN haze	12	6	5
Lmin (mW/cm^2/sr/μm)	0.4	0.4	0.5
Lmax (mW/cm^2/sr/μm)	23.8	16.4	14.2
Spectral solar irradiance	167.1	144.05	119.64
Satellite viewing angle	0	0	0
Sun elevation (°)	52.11	52.11	52.11

Table B3 Atmospheric correction parameters for 2001 image

	Band 1	Band 2	Band 3
Date (mm/dd/yy)	9/20/2001	9/20/2001	9/20/2001
Time (GMT)	14.35.04	14.35.04	14.35.04
Λ of band centre (μm)	0.565	0.66	0.825
DN haze	24	17	11
Lmin (mW/cm²/sr/μm)	-0.64	-0.5	-0.51
Lmax (mW/cm²/sr/μm)	19.65	15.29	15.74
Spectral solar irradiance	168.67		103.93
Satellite viewing angle	0	0	0
Sun elevation (°)	34.98	34.98	34.98

Table B4 Atmospheric correction parameters for 2008 image

	Band 1	Band 2	Band 3
Date (mm/dd/yy)	8/30/2008	8/30/2008	8/30/2008
Time (GMT)	15:03:47	15:03:47	15:03:47
Λ of band centre (μm)	0.565	0.66	0.84
DN haze	65	40	6
Lmin (mW/cm²/sr/μm)	0.03938	0.05332	0.06011
Lmax (mW/cm²/sr/μm)	0	0	0
Spectral solar irradiance	166.9	144.12	99.3
Satellite viewing angle	13.8	13.8	13.8
Sun elevation (°)	44.2	44.2	44.2

Radiometric calibration

A radiometric correction was applied to each image to allow for multi-date analysis. Again, the 2001 image was used as a reference to which the 1983, 2005, and 2008 images were calibrates. To begin the analysis, 25 points were digitized in homogenous areas throughout each of the images. The vector layer was then converted to a raster. Next, a linear regression was applied to each image band, whereby the independent variable represents the band being calibrated, and the dependent variable represents the corresponding band from the 2001 image. The raster of the 25 points was used as a mask.

The regression equations provide the necessary information to calibrate the images. The y-intercept corresponds to the off-set between bands, while the slope corresponds to the gain. This information applied to each band by adding the offset to the original brightness values, then multiplying by the offset. Tables B5 to B7 list the regression results for the 1983, 2005, and 2008 image.

Table B3 Radiometric calibration parameters for 1983 image

	Offset	Gain	r
Band 1	0.031907	1.69796	0.854798
Band 2	0.033563	1.843864	0.835594
Band 3	.033217	2.13184	0.870281

Table B4 Radiometric calibration parameters for 2005 image

	Offset	Gain	r
Band 1	-0.062615	0.001906	0.77574
Band 2	-0.041615	0.002595	0.805309
Band 3	-0.045349	0.004263	0.90671

Table B5 Radiometric calibration parameters for 2008 image

	Offset	Gain	r
Band 1	0.012796	0.855975	0.943391
Band 2	0.004134	0.494366	0.96842
Band 3	0.007173	0.878860	0.965917